The FEBS Journal

FEBS PRESS science publishing by scientists

The complex allosteric and redox regulation of the fumarate hydratase and malate dehydratase reactions of *Arabidopsis thaliana* Fumarase 1 and 2 gives clues for understanding the massive accumulation of fumarate

Juan P. Zubimendi[1], Andrea Martinatto[1,†], Maria P. Valacco[2], Silvia Moreno[2], Carlos S. Andreo[1], María F. Drincovich[1] and Marcos A. Tronconi[1]

1 Centro de Estudios Fotosintéticos y Bioquímicos (CEFOBI), Facultad de Ciencias Bioquímicas y Farmacéuticas, Universidad Nacional de Rosario (UNR), Santa Fe, Argentina

2 Departamento de Química Biológica, Facultad de Ciencias exactas y Naturales, Universidad de Buenos Aires (UBA), Argentina

Keywords
allosteric and redox regulation; Arabidopsis; enzyme kinetics; fumarase; paralogous genes

Correspondence
M. A. Tronconi, Suipacha 531, Rosario 2000, Argentina
Fax: +54 341 4370044
Tel: +54 341 4371955
E-mail: tronconi@cefobi-conicet.gov.ar

[†]Present address
Facultad de Ciencias Agrarias, Universidad Nacinal de Rosario (UNR), Campo Experimental Villarino, CC No 14, Zavalla, 2123, Santa Fe, Argentina

(Received 8 November 2017, revised 22 February 2018, accepted 19 April 2018)

doi:10.1111/febs.14483

Arabidopsis *thaliana* possesses two *fumarase* genes (*FUM*), *AtFUM1* (At2g47510) encoding for the mitochondrial Krebs cycle-associated enzyme and *AtFUM2* (At5g50950) for the cytosolic isoform required for fumarate massive accumulation. Here, the comprehensive biochemical studies of AtFUM1 and AtFUM2 shows that they are active enzymes with similar kinetic parameters but differential regulation. For both enzymes, fumarate hydratase (FH) activity is favored over the malate dehydratase (MD) activity; however, MD is the most regulated activity with several allosteric activators. Oxalacetate, glutamine, and/or asparagine are modulators causing the MD reaction to become preferred over the FH reaction. Activity profiles as a function of pH suggest a suboptimal FUM activity in Arabidopsis cells; moreover, the direction of the FUM reaction is sensitive to pH changes. Under mild oxidation conditions, AtFUMs form high mass molecular aggregates, which present both FUM activities decreased to a different extent. The biochemical properties of oxidized AtFUMs (oxAtFUMs) were completely reversed by NADPH-supplied Arabidopsis leaf extracts, suggesting that the AtFUMs redox regulation can be accomplished *in vivo*. Mass spectrometry analyses indicate the presence of an active site-associated intermolecular disulfide bridge in oxAtFUMs. Finally, a phylogenetic approach points out that other plant species may also possess cytosolic FUM2 enzymes mainly encoded by paralogous genes, indicating that the evolutionary history of this trait has been drawn through a process of parallel evolution. Overall, according to our results, a multilevel regulatory pattern of FUM activities emerges, supporting the role of this enzyme as a carbon flow monitoring point through the organic acid metabolism in plants.

Introduction

Fumarase [FUM (fumarase hydratase); EC 4.2.1.2)] catalyzes the reversible hydration of fumarate to L-malate. According to the amino acid sequence, subunit composition, and metal requirements, two kinds of FUMs have been identified. Class I FUMs, commonly found in prokaryotes, are homodimeric,

Abbreviations
Ala, alanine; Asn, asparagine; Asp, aspartate; CoA, coenzyme A; DAA, diamide; F1,6BP, fructose1,6BP; FH, fumarate hydratase; FUM, fumarase; Gln, glutamine; Gluc6P, glucose 6P; Glu, glutamate; LC, liquid chromatography; MDH, L-malate dehydrogenase; MD, L-malate dehydratase; MS, mass spectrometry; OAA, oxalacetate; PEP, phophoenolpyruvate; TCA, tricarboxylic acid; α-KG, α-oxoglutarate.

iron-sulfur-containing enzymes composed of subunits of 60 kDa. FUMA and FUMB from *Escherichia coli* are well-studied examples of this subgroup [1]. On the other hand, class II FUMs are tetrameric enzymes, composed of identical subunits of approximately 50 kDa, and do not have any metal requirement for activity. Class II FUMs are the typical FUMs of eukaryotic organisms; although they have also been found in prokaryotes (e.g., FUMC from *E. coli*; [1]). Class I and class II FUMs exhibit a low degree of sequence homology and it seems that they have been originated from different ancestors: an aconitase-like and aspartase-like ancestor, respectively [2]. Thus, fumarase activity represents an example of convergent functional evolution.

The crystal structures of *E. coli* FUMC [3] and fumarase from yeast [4] and human [5] were resolved. The three proteins share a primary structure identity of about 70% and each monomer is composed of three mainly α-helical domains (D1, D2, and D3), with the active site located in the cleft of D1 and D3. Three conserved regions (C1, C2, and C3), separated from each other in the monomer, gather from three different subunits to form one active site. Part of region C3 is a flexible loop (the 'SS loop') of the active site and contains the signature sequence GSSXXPXKXN that defines the aspartase/fumarase superfamily [6].

FUM participates in the tricarboxylic acid (TCA) cycle; therefore, it is found within mitochondria in eukaryotic organisms. Despite this ubiquitous subcellular localization, FUM has also been found in the cytosol of fungi and animal cells. In these organisms, cytosolic and mitochondrial fumarases are encoded by a single gene (they have been named *echoforms*: identical proteins in different subcellular compartments) [7]. The detailed mechanism for this dual targeting is still under investigation but it may depend on the organism [8,9]. Moreover, cytosolic FUM moves to the nucleus following either hydroxyurea or ionized radiation treatments in HeLa lines and yeast cells. FUM activity is required for the localized synthesis of fumarate which, in turn, acts as a secondary messenger, or as an enzymatic cofactor, in the signaling pathway that leads to double-stranded DNA break repair [10].

In plants, *Arabidopsis thaliana* is the only species in which the presence of a cytosolic FUM has been proved to date [11]. Unlike fungi and animals, *A. thaliana* possesses two *FUM* genes: *AtFUM1* (At2g47510), which encodes for the mitochondrial isoform; and *AtFUM2* (At5g50950) for the cytosolic fumarase [11]. As expected by its role in the TCA cycle, *AtFUM1* is an essential gene; however, *AtFUM2,* which accounts for the major fumarase activity measured in Arabidopsis leaves, is mainly required for the massive fumarate accumulation during the day in plants grown under high nitrogen (N) [11]. This fact suggests that AtFUM2 acts in the direction of fumarate synthesis [L-malate dehydratase (MD) activity] during the N-rich autotrophic phase. However, at night, when the stored fumarate is mobilized for replenishing TCA intermediates and for respiration [12,13], AtFUM2 would run in the opposite direction [fumarate hydratase (FH) activity], to support the heterotrophic growth stage. It has been demonstrated that L-malate dehydrogenase (MDH) protein abundance and AtFUM1 activity are increased during the day in Arabidopsis [14], and thus, AtFUM1 could act in concert with AtFUM2 for the accumulation of fumarate through a reductive branch of the TCA cycle [15]. However, the physiological roles proposed for the Arabidopsis FUMs are hindered by the lack of information on the kinetic and regulatory properties of plant FUMs.

Here, we present the biochemical characterization of the two FUM isoforms from *A. thaliana*. Both FUMs were kinetically analyzed in the two directions of the reaction, and the allosteric and redox modulation of both activities were characterized. Based on the results, a model of AtFUMs activity regulation exerted by the coordinated action of organic and amino acids, and by the redox state, emerges. Overall, this work gives clues for understanding the direction of the carbon flux through the FUM reaction, which depends on the particular Arabidopsis FUM isoform and it is exerted at different levels of activity modulation.

Results

Cloning and *in silico* analysis of Arabidopsis FUMs

In Arabidopsis, *AtFUM1* encodes a single transcript for the mitochondrial enzyme, while *AtFUM2* encodes two different transcripts produced by an alternative splicing of the primary transcript, which were called *AtFUM2* and *AtFUM2b* (www.arabidopsis.org). The full-length cDNAs for the mature (without targeting peptide) AtFUM1 and for the cytosolic AtFUM2 and AtFUM2b were cloned using RNA from Arabidopsis leaf. AtFUM2 possesses 32 amino acid residues at the N-terminal region, which are not present in AtFUM1 [11]. On the other hand, AtFUM2 and AtFUM2b proteins differ at their C-terminal region. Here, AtFUM2b presents 40 amino acid residues with no homology with other FUMs described to date because the last intron is retained in AtFUM2b transcript

(Fig. 1A). The alternative splicing results in mRNAs with a premature termination codon and, thus, AtFUM2b lacks the sequence encoded by the last exon (Fig. 1A). Despite these differences, the three putative FUMs share 86–94% identity at the amino acid level and possess the three C1, C2, and C3 conserved motives found in other class II FUMs [6].

The AtFUM1 and AtFUM2 full-length coding DNA sequences (CDS) were used to construct a phylogenetic tree, along with the CDS of *FUM* genes from Viridiplantae species (Fig. 2). Programs for alternative translation initiation sites (TIS) and protein subcellular localization (see 'Experimental Procedures') indicated that several plant species have a specific gene for cytosolic FUM (hereafter *FUM2*) (Fig. S1). In the Brassicaceae family (crucifers), putative *FUM2* genes are found in species of Lineage I (*Arabidopsis lyrata*, *Capsella rubella*, *Camelina sativa*, and *Boechera stricta*), but not in species of Lineage II (*Thellungiella parvula*, *Eutrema salgsugineum*, *Sisymbrium irio*, and *Brassica* spp.) or in the 'basal Lineage' of crucifers represented by *Aethionema arabicum* (Fig. 2). Even in Lineage I,

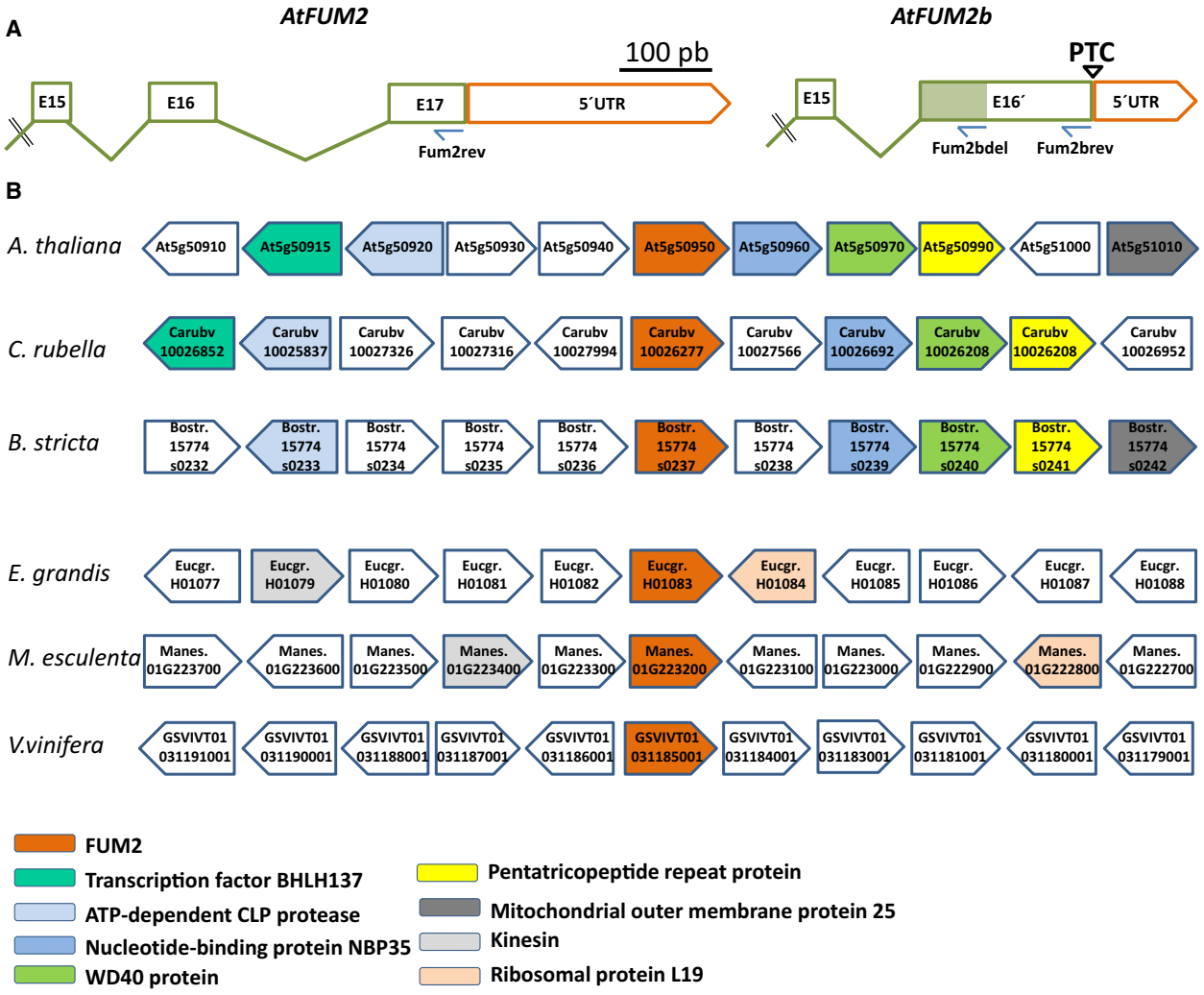

Fig. 1. *In silico* analyses of *AtFUM1* and *AtFUM2*. (A) Schematic representation of 3′ region of *AtFUM2*. Exons (E) are represented by green rectangles and introns are symbolized by thin green lines. The 3′ UTRs (untranslated regions) are represented by orange rectangles. The green box indicates the E16 of AtFUM2 transcript on AtFUM2b sequence. The two mRNA variants differ in the last intron, which is retained in AtFUM2b generating a protein that lacks the amino acid residues encoded by E17 as consequence a premature termination codon (PTC). Positions of reverse primers for full-length cDNA amplification of AtFUM2, AtFUM2b, and AtFUM2bdel are shown as arrows. (B) Flanking genes of *FUM2* in *A. thaliana*, *C. rubella*, *B. stricta*, *E. grandis*, *M. sculenta*, and *V. vinifera*. Arrows with the same color indicate genes with the same putative function. Genes in white do not have orthologs in the regions analyzed. Genes ID from sequencing projects are indicated in each case.

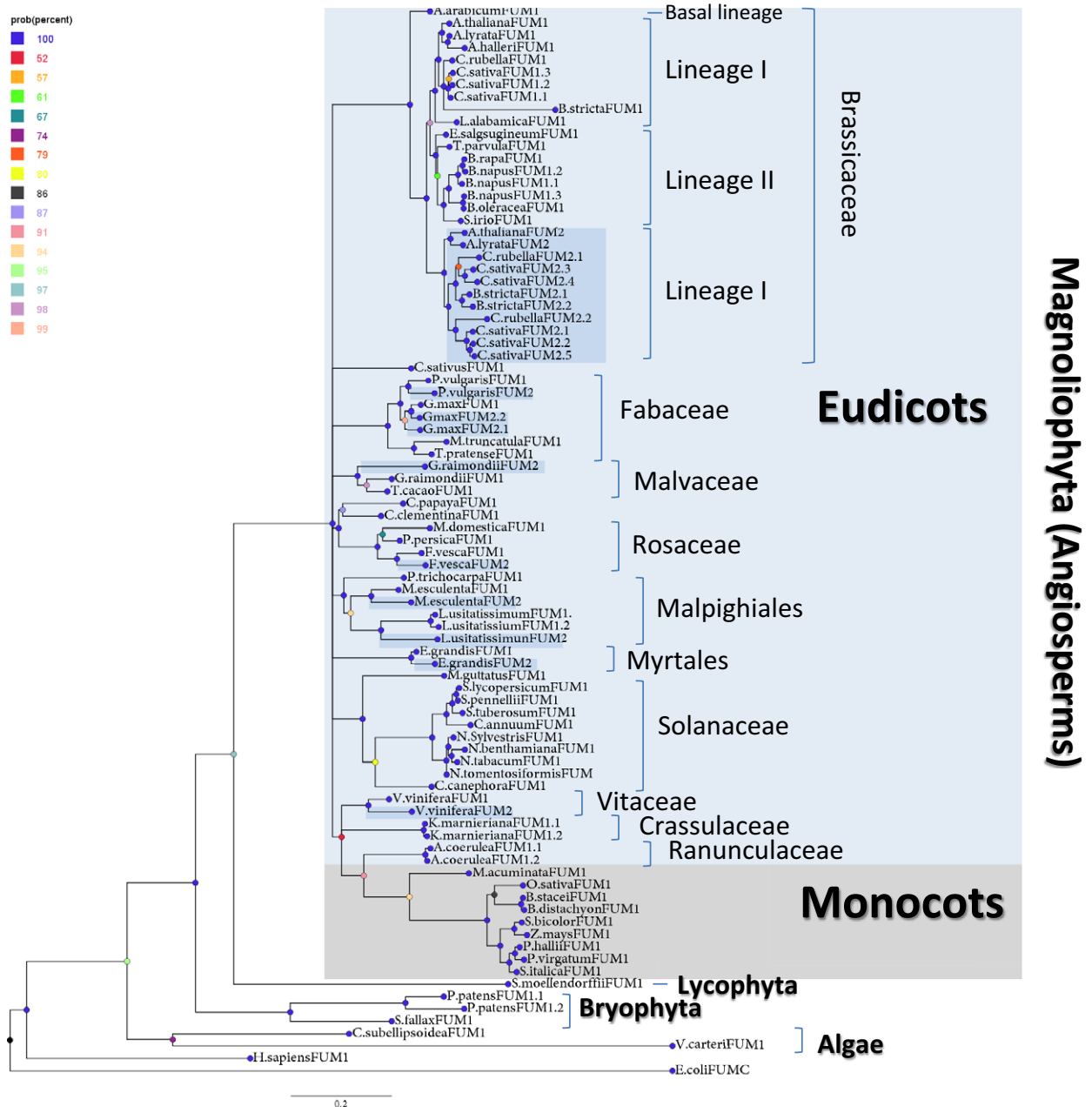

Fig. 2. Phylogenetic tree of plant FUM full-length coding DNA sequences. Evolutionary history was inferred by using the Bayesian method based on the GTR + G (0.739) + I (0.160) evolutionary model. The 50% majority-rule consensus tree is shown. The tree is drawn to scale, with branch distance separating two taxes measured considering the number of substitutions per site. Sequences are named according to the species and FUM isoform. FUM2s are shaded in light blue. Colored spheres that connect taxes represent BPP values according to the scale on the left of the Figure. Brasicaceae Lineages I and II are referred according to Ref. [44]. In *C. sativa*, the number of total *FUM* genes is several times higher than that of *A. thaliana* as a consequence of its hexaploid genome structure. *B. stricta* and *C. rubella* present additional copies of *FUM2*.

FUM2 penetrance would not be exhaustive, as *Arabidopsis halleri* and *Leavenworthia alabamica* lack *FUM2* gene. Crucifer *FUM2s* group together, constituting a separated cluster from *FUM1*. The genomic flanking sequences of *FUM2* in *A. thaliana*, *C. rubella*, and *B. stricta,* indicates that they are orthologs in these species (Fig. 1B). Outside the crucifer family, *Vitis vinifera*, *Manihot esculenta*, *Linum usitatissimum*, *Phaseolus*

vulgaris, *Glycine max*, *Fragaria vesca*, *Eucaliptus grandis*, and *Gossypium raimondii* also have, at least, one gene for a cytosolic FUM (Fig. 2). In these species, *FUM2* forms species-specific clusters with the *FUM1* sequence, instead of clustering together as in Brassicaceae (Fig. 2). Besides, the coding flanking genomic regions of some of these *FUM2* genes show no homology (Fig. 1B), and, thus, they could thus be assigned as paralogs. We further analyzed this possibility in the clade that groups *G. max* and *P. vulgaris* by calculating the rate of synonymous substitutions (K_s) for *FUM1* and *FUM2* gene pairs. Ks values for the *FUM* gene pairs were much lower than 0.283 (see 'Experimental Procedures' and Table S1), which indicates that the *FUM2* sequence is a species-specific paralogous gene in this clade. Interestingly, none of the monocot genomes predicts a cytosolic FUM2 (Fig. 1B). Besides, several Viridiplantae species have extra copies of *FUM1* gene (Fig. 2). Overall, these *in silico* studies indicate that in plants, FUM family constitution is highly species-dependent.

A similar N-terminal sequence to that found in AtFUM2 (and -2b) is also present in orthologs from *A. lyrata*, *C. rubella, C. sativa*, and *B. stricta*, but not in other cytosolic FUMs (Fig. S1). The analysis of the sequence encoding for this extended N-terminal region indicates a threefold higher substitution nucleotide rate than that for the complete CDS with the most common substitutions being transversions (not shown). This rate of change is similar to that shown by 5′ UTR of *FUM2* genes (not shown). Thus, the exclusive N-terminal sequence of Brassicaceae FUM2 would not be associated to the enzymatic function.

Purification and biochemical characterization of recombinant AtFUMs

AtFUM1, AtFUM2, and -2b were expressed as recombinant proteins in *Escherichia coli*. Proteins with the expected molecular masses of 54 kDa for AtFUM1 and 58 kDa for AtFUM2 and AtFUM2b were purified to homogeneity (Fig. 3A). The electrophoretic mobility of the three recombinant AtFUMs in nondenaturing PAGE is consistent with a tetrameric oligomeric state (Fig. 3B). Native PAGEs revealed by fumarase activity indicate that only AtFUM1 and AtFUM2 are active FUM enzymes (Fig. 3B). The mobility of recombinant AtFUMs is similar to that exhibited by the enzyme present in Arabidopsis leaf extracts (Fig. 3B). The oligomeric state of AtFUMs was confirmed by gel-filtration chromatography. At pH 8, AtFUM1, AtFUM2, and -2b eluted as simple peaks, which corresponded to a molecular mass of 195 ± 20, 216 ± 15, and 220 ± 22 kDa, respectively.

Kinetic characterization of AtFUM1 and AtFUM2

Recombinant purified AtFUM1 and -2 showed both FH and MD activities and were kinetically characterized (Table 1). However, we were unable to detect any activity for AtFUM2b, even for a synthetic variant of this isoform lacking the forty amino acidic residues encoded by the 3′ unspliced sequence in AtFUM2b transcript (Fig. 1A). We suggest that the lack of enzymatic activity of AtFUM2b is probably due to the absence of residues encoded by the last exon, which, as we will discuss later, are part of the active site.

The activity of AtFUM1 and -2 was measured at different pH values to determine the optimum pH for the FH and MD reactions. For AtFUM1, the highest activity in both directions of the reaction was at pH 8.0. However, in the case of AtFUM2, different pH optimum was found for the FH and MD reactions; pH 7.7 for the FH reaction, and 8.2 for the MD activity (Table 1). For the FH reaction, both enzymes were active in a broad range of pH; in contrast to the MD reaction, with a more drastic drop of activity below and above the optimum pH (Fig. 4A, B). Thus, at physiological pH values (7.0–7.3), FH activity is almost 70% of that measured at the optimum pH and about four times higher than MD activity (Fig. 4A).

AtFUM1 and 2 displayed typically hyperbolic substrate saturation curves for both directions of the reaction (Fig. 4C,D). AtFUM1 exhibited 1.3-fold higher V_{max} for the FH reaction than for the MD reaction (Table 1). The K_m values for the substrates were in the millimolar order, and the affinity for fumarate was 2.6-fold higher than that for L-malate (Table 1). Hence, the FH to MD catalytic efficiency ratio for AtFUM1 was 3.5 (Table 1).

Since AtFUM2 exhibited different optimum pH for the FH and MD reactions, we determined the kinetic parameters at their optimum pH, at the optimal pH value of the opposite reaction, and at pH 8 (optimum pH of AtFUM1) (Table 1). For the FH reaction, the shift of pH above the optimum (7.7) slightly decreases the V_{max} without significant changes in the K_m value (Table 1). In turn, for the MD reaction, the shift of pH below its optimum (8.2) caused a marked decrease in both the maximum activity and the K_m values (Table 1). However, at pH 8, the MD reaction of AtFUM2 retained almost 95% of the total activity without significant changes in the affinity for L-malate. Thus, the subsequent kinetic characterization of AtFUM2 was performed at pH 8. AtFUM2 showed

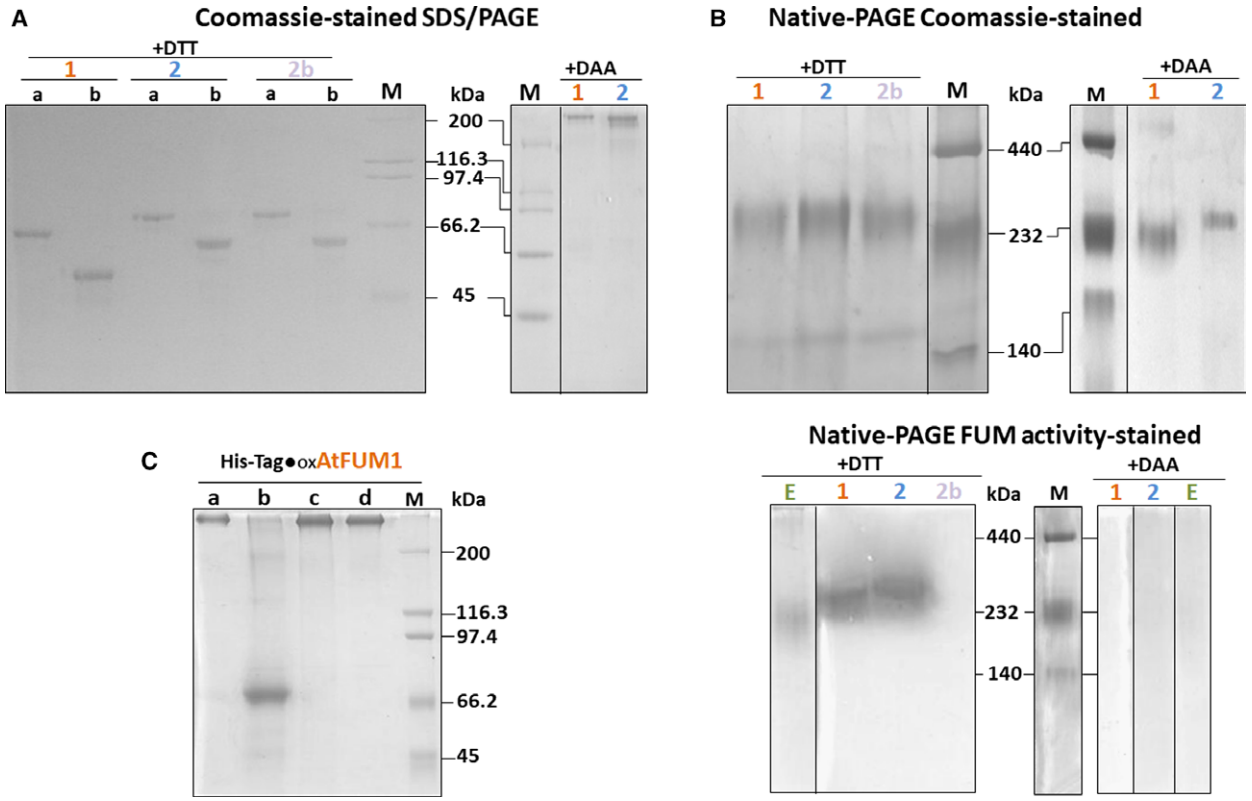

Fig. 3. Recombinant AtFUM1, AtFUM2, and AtFUM2b isoforms analyzed by gel electrophoresis. (A) Coomassie-stained SDS/PAGEs: 5 μg of His-tag (rows a) or thrombin-digested (rows b) AtFUM1 (1), AtFUM2 (2) and AtFUM2b (2b) were incubated with 2 mM DTT or 2 mM DAA prior to PAGE under nonreducing conditions (without addition of 2-mercaptoethanol to the Laemmli Sample Buffer). (B) Nondenaturing PAGEs: 10 μg (for Coomassie-stained gels) or 0.5 μg (~30 milliunits, for FUM activity-stained gels) of AtFUM1 (row 1), AtFUM2 (row 2), and AtFUM2b (row 2b) were loaded after treatment with 2 mM DTT or 2 mM DAA. A DTT-reduced or DAA-oxidized Arabidopsis leaf extract (20 milliunits) was also loaded on the FUM activity-stained gel. (C) His-Tag oxAtFUM1 was bound to the Ni-NTA matrix and the protein eluted after different treatments was analyzed by Coomassie-stained SDS/PAGE under nonreducing conditions. Row 1, eluted protein without any treatment; Row 2, after incubation with Arabidopsis leaf extract and 100 μM NADPH; Row 3, after incubation with Arabidopsis leaf extract; Row 4, after incubation with 100 μM NADPH. M: Molecular weight marker (M).

Table 1. Kinetic parameters of AtFUM1 and AtFUM2. The indicated values, obtained by nonlinear regression, are the average (± SD) of at least three different measurements. In the case of AtFUM1, the parameters obtained at optimum pH (8.0) are indicated. In the case of AtFUM2, parameters at optimum pH for FH reaction (7.7) and for MD reaction (8.2), as well as at pH (8.0), are shown.

	FH activity				MD activity				FH to MD
	pH	V_{max} (U·mg^{-1})	K_m (mM)	k_{cat}/K_m (s^{-1}·mM^{-1})	pH	V_{max} (U·mg^{-1})	K_m (mM)	k_{cat}/K_m (s^{-1}·mM^{-1})	efficiency ratio
AtFUM1	8.0	75.0 ± 3.9	0.7 ± 0.1	30.0	8.0	55.0 ± 1.3	1.8 ± 0.2	8.5	3.5
AtFUM2	7.7	77.5 ± 5.0	0.4 ± 0.1	57.6	7.7	17.9 ± 2.0	0.6 ± 0.1	8.7	6.6
	8.0	74.5 ± 3.0	0.5 ± 0.1	44.3	8.0	49.5 ± 3.5	1.7 ± 0.3	8.7	5.1
	8.2	66.5 ± 4.0	0.5 ± 0.2	36.6	8.2	57.3 ± 6.0	1.9 ± 0.2	9.0	4.0

3.4-fold higher affinity for its substrate and 1.5 times higher maximum activity in the FH than in the MD direction (Table 1). Then, the FH to MD catalytic efficiency ratio was 5.1 for AtFUM2 at pH 8 (Table 1).

A hyperbolic kinetic response with a K_m value for fumarate of 0.6 mM was obtained when FH activity was measured on desalted leaf Arabidopsis extracts in the presence of increasing fumarate concentrations (Fig. 4E). This value is in the order of those calculated for the recombinant AtFUMs, suggesting that the heterologous expression strategy resulted in well-structured proteins.

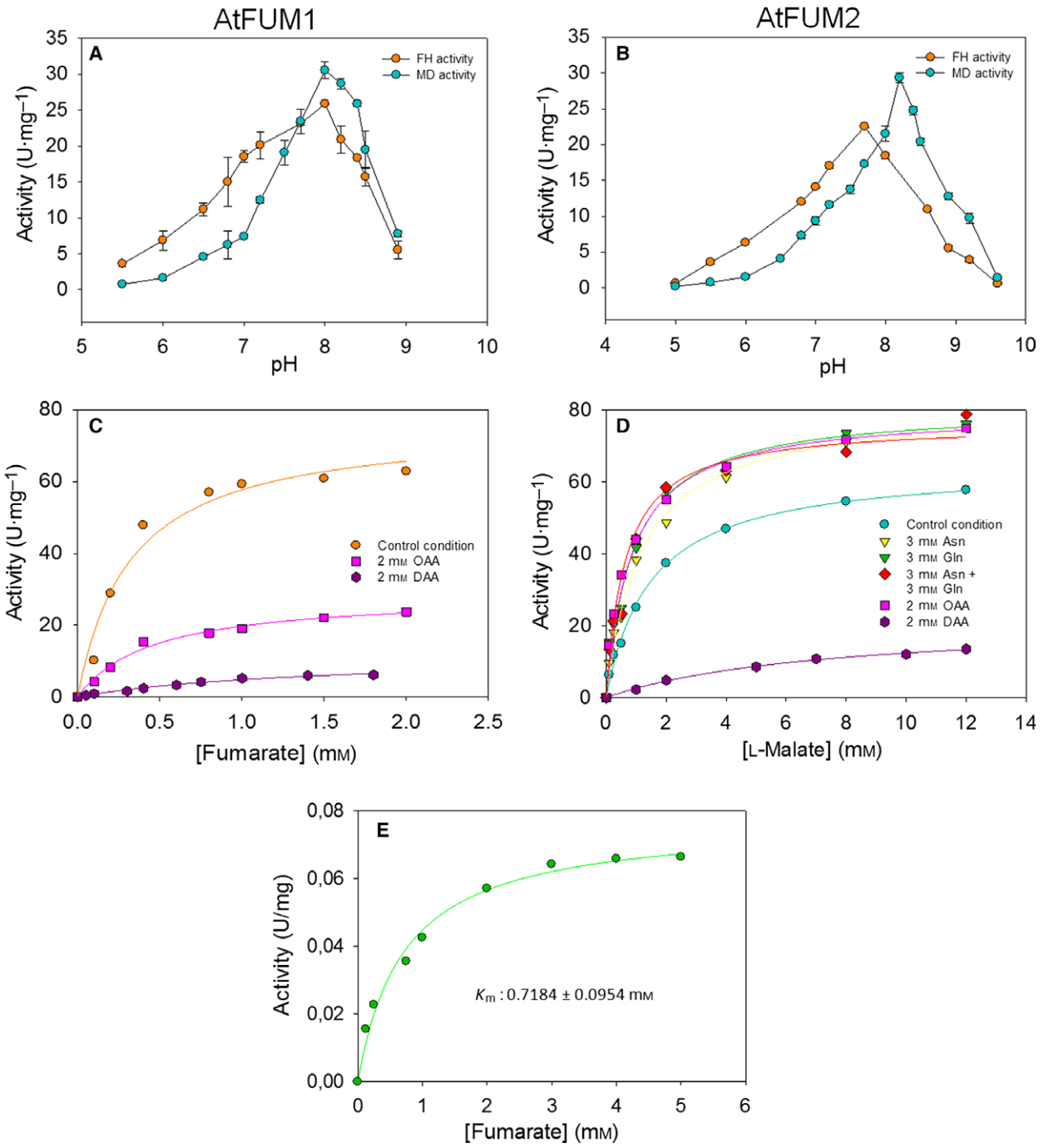

Fig. 4. Optimum pH and substrate saturation curves. Profiles of activity versus pH of AtFUM1 (A) and AtFUM2 (B). The FH and MD activities were determined using the standard assay method at nonsaturating levels of substrates (0.5 mM fumarate or 1.5 mM L-malate) at different pH values. Assays were done at least in triplicate and error bars indicate SD. Effect of substrate concentration on the FH activity of AtFUM1 (C) and MD activity of AtFUM2 (D). The FH and MD activities were determined at different concentrations of L-malate or fumarate, respectively, at pH 8. In both cases, the effect of a fixed amount of an allosteric effector or a redox agent is shown. Control condition refers to kinetic determinations without the addition of any modulator. (E) Effect of fumarate concentration on the FUM activity of Arabidopsis leaf extracts. The kinetic determination was carried out through the NADP-ME reaction coupled assay. The K_m value of isoforms present in the leaf extracts is shown in the plot. Typical results from at least three independent determinations are shown in (C), (D), and (E).

Regulatory properties of AtFUM1 and AtFUM2

Several intermediates of glycolysis: glucose-6P (Gluc6P); fructose1,6BP (F1,6BP); phophoenolpyruvate (PEP); and pyruvate; and of the TCA cycle: citrate; α-oxoglutarate (α-KG); succinate; oxaloacetate (OAA); coenzyme A (CoA); and acetyl-CoA; as well as amino acids (Ala, Glu, Asp, Gln, and Asn), adenilates (ATP and ADP), and metals (Mg^{+2} and Mn^{+2}) were tested as possible effectors of the AtFUMs activity. The activities were assayed with nonsaturating concentrations of the substrates L-malate or fumarate.

Regulation of the FH activity at pH 8

The FH activity of AtFUM1 and AtFUM2 was strongly inhibited by phophoenolpyruvate, citrate, OAA, ATP, and ADP (Table 2). Both isoforms showed similar sensitivity to these compounds, with $Ki_{(app)}$ values that were in the range of 0.03–1.9 mM. Interestingly, although both ATP and ADP decreased FH activity, ATP was a more efficient inhibitor, with a $Ki_{(app)}$ value over fivefold lower than $Ki_{(app)}$ for ADP. The effect of other effectors depended on the isoform considered. In this regard, pyruvate and α-KG behaved as inhibitors of AtFUM2, while Glu6P acted as activator of AtFUM1 (Table 2).

Regulation of the MD reaction at pH 8

The MD reaction of AtFUMs was more susceptible to allosteric modulation than the reverse reaction, with several intermediates that acted as activators (Table 2). OAA, Asn, and Gln positively modulated AtFUM1 and AtFUM2 activities with similar $Ka_{(app)}$ values for both enzymes. In addition, pyruvate and phophoenolpyruvate behaved as activator and inhibitor of AtFUM1, respectively, but did not modify AtFUM2 activity. On the other hand, while citrate, succinate, ADP, and ATP acted as inhibitors of both AtFUMs, Gluc6P only inhibited AtFUM1. For both enzymes, citrate, phophoenolpyruvate, and ATP were weaker inhibitors for the MD reaction than for the FH reaction (Table 2). In contrast, ADP was a stronger inhibitor for the MD reaction than for the FH one ($Ki_{(app)}$ fourfold lower, Table 2).

F1,6BP, CoA, acetyl-CoA, Ala, Asp, and Glu, assayed at 0.5 and 2 mM, did not significantly modify AtFUM1 and AtFUM2 activity, neither the FH nor the MD reaction. Bivalent cations, Mg^{+2} and Mn^{+2}, slightly inhibited the reactions of both enzymes at concentrations higher than 2 mM (not shown).

Finally, the modulators considered the most relevant were checked at pH 7.2 (Table S2). In general, there were no changes in the effect on FUM activity at this pH. The exception was Glu, which behaved as an activator of the MD activity of AtFUM1 and Asp, which showed the same effect on AtFUM2 (Table S2). OAA did not inhibit the FH activity of AtFUM2 at pH 7.2, either (Table S2).

Kinetic parameters of AtFUM1 and AtFUM2 in the presence of effectors

The effect of 3 mM OAA, Asn, and Gln on kinetic parameters of AtFUM1 and -2 activities was analyzed

Table 2. Regulatory properties of AtFUM1 and AtFUM2. Activities were measured at pH 8.0 in the absence or presence of each effector. Fumarate and L-Malate concentration were kept at the Km/3 value (Table 1). The results represent the % of activity in the presence of saturating concentrations of the effectors in relation to the activity measured in the absence of the metabolites (100%). The value is the average of at least three determinations, with an SD value lower than 5%. A: significant activation (more than 130%); I: significant inhibition (less than 70% residual activity); H, hyperbolic behavior; S, sigmoidal behavior; NM, no modulation.

	AtFUM1						AtFUM2					
	FH activity			MD activity			FH activity			MD activity		
Metabolite	Effect	Activity (%)	$K_{(app)}$ (mM)	Effect	Activity (%)	$K_{(app)}$ (mM)	Effect	Activity (%)	$K_{(app)}$ (mM)	Effect	Activity (%)	$K_{(app)}$ (mM)
Gluc6P	A	180	1.9(S)	I	13	0.8(S)	NM		–	NM	–	–
Phophoenolpyruvate	I	23	0.6(H)	I	17	1.2(S)	I	21	0.7(H)	NM	–	–
Pyr	NM	–	–	A	178	2.4(S)	I	15	1.6(H)	NM	–	–
Citrate	I	15	0.8(S)	I	32	2.9(H)	I	31	0.5(H)	I	37	2.6(H)
Succinate	NM	–	–	I	20	2.9(H)	NM	–	–	I	37	1.1(H)
α-KG	NM	–	–	NM	–	–	I	22	0.8(H)	NM	–	–
OAA	I	14	0.8(S)	A	190	1.1(H)	I	14	1.2(S)	A	177	1.2(S)
Asn	NM	–	–	A	170	1.2(S)	NM	–	–	A	175	0.8(S)
Gln	NM	–	–	A	188	1.1(S)	NM	–	–	A	182	1.1(H)
ATP	I	8	0.03(S)	I	10	0.16(H)	I	13	0.03(S)	I	19	0.3(H)
ADP	I	12	0.16(H)	I	7	0.04(S)	I	24	0.2(S)	I	13	0.06(S)

at pH 8. These compounds did not affect the substrate kinetic behavior (Fig. 4C,D). For the FH reaction, OAA behaved as an inhibitor of AtFUM1 and -2 by decreasing about four times the V_{max} without significant changes in the K_m for L-malate (Table 3). For the MD reaction, this metabolite stimulated the activity, increasing the V_{max} and the affinity for the fumarate, albeit to different extents. Overall, OAA is able to shift the direction of FUM reaction, favoring the MD over the FH reaction for both isoenzymes.

The presence of either 3 mM Asn or 3 mM Gln had practically the same effect on the kinetic parameters for the MD reaction of AtFUM1 and 2 (Table 3). The V_{max} increased up to twofold while the affinity for fumarate increased more than three times. Hence, the MD reaction was favored over the FH in the presence of 3 mM Asn or Gln. Synergistic or additive effect of these activators was not observed, suggesting that Asn and Gln interact at a common allosteric site (Table 3).

Redox modulation of recombinant AtFUM1 and AtFUM2

Purified recombinant proteins were incubated with diamide (DAA), a chemical oxidant widely used to induce the formation of disulfides [16]. A time-dependent decrease of FH and MD activity in the presence of 2 mM DAA was registered (Fig. 5). The two enzymes reached nearly 20% of the initial activity at 70 min of incubation for both directions of the reaction. When the activity reached the minimum value, 2 mM DTT was added to the enzymes and a complete recovery of the initial activity was observed for AtFUM1 and AtFUM2 (Fig. 5A, B). Increased concentrations of DAA or DTT modified the time required to reach the plateau without changes in the final activity values (not shown). A similar time-dependent inactivation/activation behavior was observed for the FH activity measured on desalted leaf Arabidopsis extracts treated with 2 mM DAA and subsequent addition of 2 mM DTT (Fig. 3B).

Kinetic and structural properties of oxidized and reduced AtFUM1 and AtFUM2

The kinetic parameters of DAA-treated AtFUM1 and -2 were determined at pH 8 for both directions of the reaction. For this, the enzymes were incubated with 2 mM DAA for 90 min at 0 °C and the treated enzymes [oxidized AtFUM (oxAtFUM)] used for kinetic measurements. The oxidation causes a reduction of AtFUM1 and -2 maximum activities and an increase in K_m for the substrates (Table 3), without changes in the shape of the saturation curves (Fig. 4C, D). For the FH reaction, this led to a nearly 15-fold decrease of the catalytic efficiency for both oxAtFUM1 and -2 (Table 3). Conversely, the MD catalytic efficiency of AtFUM1 and -2 was differentially affected by DAA treatment, with a 28-fold and 2.5-fold decrease, respectively (Table 3).

The oligomeric state of oxAtFUM1 and -2 was analyzed by nondenaturing PAGE. The enzymes incubated with DAA show the same mobility in

Table 3. Kinetic parameters of AtFUM1 and AtFUM2 in the presence of metabolic effectors and after oxidation. All assays were conducted at pH 8.0 in the presence of 3 mM Asn or/and Gln; or 3 mM OAA. The oxidation of AtFUM (oxAtFUM) was performed by preincubation with 2 mM DAA for 90 min. N.M: not modified. The fold change is expressed as the relation of k_{cat}/K_m in the presence of the effector in relation to the k_{cat}/K_m without effector. The values are the average (± SD) of at least three determinations.

		FH activity				MD activity				
	Additions	V_{max} ($U \cdot mg^{-1}$)	K_m (mM)	k_{cat}/K_m ($s^{-1} \cdot mM^{-1}$)	Fold change	V_{max} ($U \cdot mg^{-1}$)	K_m (mM)	k_{cat}/K_m ($s^{-1} \cdot mM^{-1}$)	Fold change	FH to MD efficiency ratio
AtFUM1	–	75.0 ± 3.9	0.7 ± 0.1	30.0	–	55.0 ± 1.3	1.8 ± 0.2	8.5	–	3.5
	+OAA	28.7 ± 2.0	0.5 ± 0.1	8.5	0.3	70.0 ± 5.0	0.5 ± 0.2	37.0	4.6	0.2
	+Asn	N.M	N.M	N.M	–	89.1 ± 4.3	0.6 ± 0.2	41.3	4.9	0.7
	+Gln	N.M	N.M	N.M	–	88.0 ± 6.0	0.6 ± 0.1	41.0	4.7	0.7
	+Asn +Gln	N.M	N.M	N.M	–	94.2 ± 2.2	0.5 ± 0.1	52.3	6.0	0.5
	oxAtFUM	10.3 ± 0.7	1.4 ± 0.2	2.0	0.07	6.2 ± 2.0	6.3 ± 0.3	0.3	0.04	6.6
AtFUM2	–	74.5 ± 5.0	0.5 ± 0.1	44.3	–	49.5 ± 3.5	1.7 ± 0.3	8.7	–	5.1
	+OAA	16.0 ± 0.8	0.5 ± 0.2	9.7	0.2	76.0 ± 4.0	0.6 ± 0.1	37.8	4.3	0.3
	+Asn	N.M	N.M	N.M	–	97.0 ± 4.0	0.5 ± 0.1	57.7	6.6	0.7
	+Gln	N.M	N.M	N.M	–	98.0 ± 5.0	0.4 ± 0.2	73.0	8.4	0.6
	+Asn+Gln	N.M	N.M	N.M	–	99.0 ± 6.0	0.4 ± 0.1	78.2	8.6	0.5
	oxAtFUM	13.0 ± 2.0	0.7 ± 0.2	5.1	0.1	28.1 ± 4.0	2.4 ± 0.3	3.6	0.4	1.4

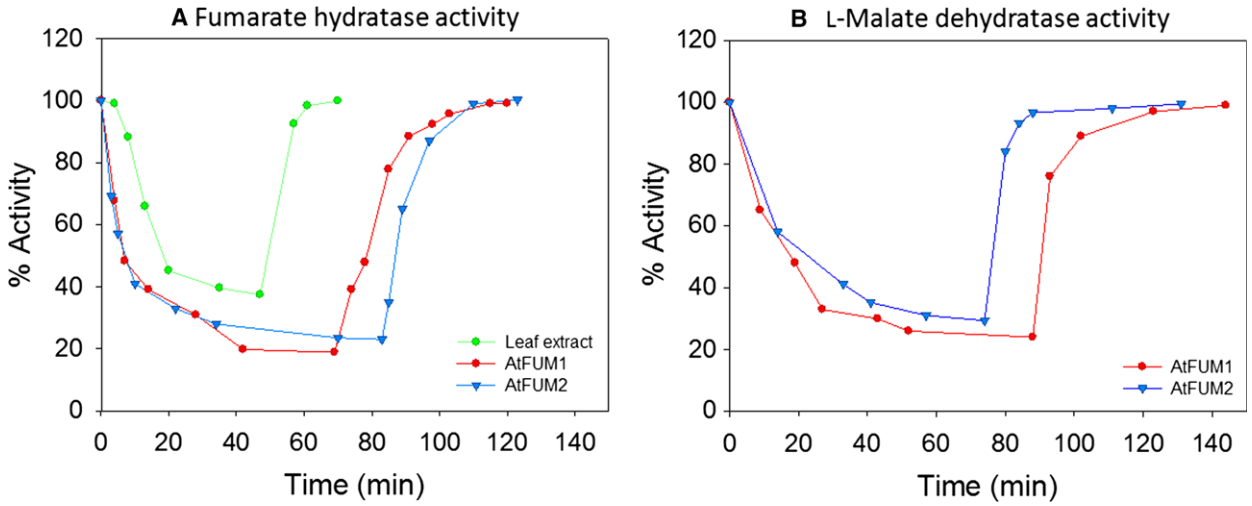

Fig. 5. Redox modulation of AtFUMs. Recombinant AtFUM1 and AtFUM2 were incubated with 2 mM DAA and FH (A) and MD (B) activities were measured at several time points and expressed as a percentage of the initial activity. When the activities reached a minimum value, the AtFUMs were further incubated with 2 mM DTT, and the activity was measured until a maximum plateau value was reached. The same assay was carried out on Arabidopsis leaf extracts and the FH reaction (A) was registered through the NADP-ME coupled assay. Typical results from at least three independent determinations are shown.

Coomassie-stained native electrophoresis as the proteins treated with DTT (reAtFUMs), with a molecular mass consistent with a tetrameric assembly (Fig. 3B). However, when oxAtFUM1 and oxAtFUM2 were analyzed by SDS/PAGE under nonreducing conditions (without addition of 2-mercaptoethanol to the Laemmli Sample Buffer), both enzymes migrated as high mass molecular aggregates in the size range of 200 kDa (Fig. 3A), suggesting that intersubunit covalent interactions were generated by DAA treatment.

Finally, we evaluated whether the reduction of oxAtFUMs could be accomplished by incubation with Arabidopsis leaf extracts. For this, the oxAtFUM1 was incubated with Arabidopsis crude leaf extracts, in the presence or the absence of NADPH. The treated enzyme was analyzed by Coomassie-stained SDS/PAGE under nonreduction conditions (Fig. 3C). Our results indicate the oxAtFUM1 is reduced by incubation with the leaf extract and 100 μM NADPH, but not by the extract or NADPH alone (Fig. 3C).

Mass spectrometry of oxidized and reduced AtFUM2

Based on the results shown here, intermolecular disulfide bridges in the tetrameric assembly oxAtFUMs are speculated. In this regard, the predicted three-dimensional model of AtFUM2 suggests that Cys252 and Cys339 would be close enough to the corresponding residues of two different monomers to be involved in Cys252-Cys252 and Cys339-Cys339 intermolecular disulfide bridges in the homotetrameric assembly (Fig. 6). In order to confirm this, an LC–MS-based mass spectrometry (MS) analysis of tryptic peptides of reAtFUM2 and oxAtFUM2 was carried out. Gel slices including the protein bands were excised from Coomassie-stained nonreducing SDS/PAGE and treated with iodoacetemide (IAM) to block thiol groups prior to digestion with trypsin. Hence, the pattern of peptides obtained for blocked re- and oxAtFUM2 was analyzed to detect differences. PROTEIN PROSPECTOR software (University of California, San Francisco, CA, USA) was used for the *in silico* calculation of the m/z ratio of AtFUM2 peptides after trypsin digestion in order to assign IAM-modified cysteine-containing peptides or disulfide-linked dipeptides. Analysis of the MS spectra showed peaks corresponding to the mass of homodipeptides between Cys339 (Table S3C). The sequence of these dipeptides was verified by MSMS fragmentation (Table S3D, E). In addition, a peptide containing Cys339 with a Δ mass + 57 Da (corresponding to carbamidomethyl group added to thiols) was observed in reAtFUM2 sample. Although this peak was not present in oxAtFUM2 (Table S3A, B), the non-carbamidomethylated form was observed, indicating the presence of some free Cys339 in this sample. Also, a Cys252-containing peptide with a Δ mass + 57 Da was found in reAtFUM2 sample (Table S3A, B). However, it was not possible to identify the corresponding homodipeptide in the oxAtFUM2 sample.

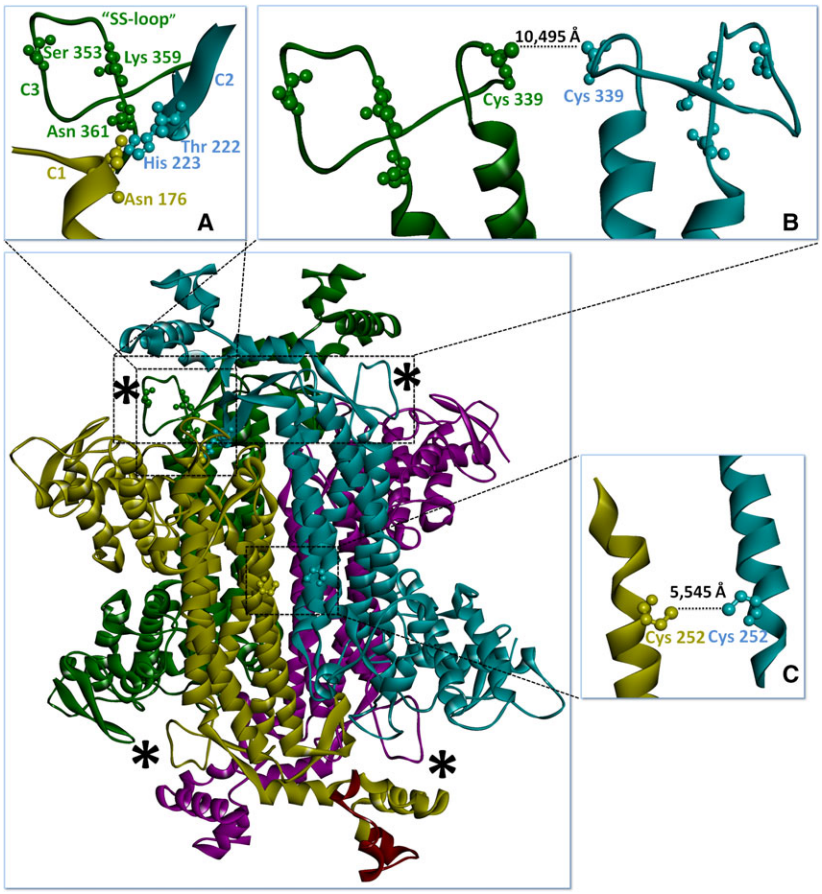

Fig. 6. Three-dimensional model view of AtFUM2 quaternary structure. The predicted model was obtained with the protein structure homology-modeling server (SWISS-MODEL; http://expasy.ch/swissmod/SWISS-MODEL.html) and fitted to recombinant yeast fumarase (PDB ID: 1YFM). Modifications were made with Discovery Studio Visualizer v16.1.0.15350. Each monomer of the tetramer is shown in a different color (magenta, light blue, yellow, and green). The black asterisks indicate the region where each active site is located. At the bottom of the structure, the C-terminal region coded by the exon 17 of *AtFUM2* gene, not present in the AtFUM2b protein, is shown in red. Particular regions of the global AtFUM2 structure are shown in separated *A*, *B*, and *C* boxes. A, One active site is constituted by three C1, C2, and C3 conserved regions, each provided by different monomers. The amino acid residues involved in the catalysis are represented as sticks and spheres. B and C, The Cys residues that form intermolecular disulfide bridges. There are two Cys252-Cys252 and Cys339-Cys339 arrangements in the quaternary structure. Relative distances between Cys residues are indicated in Angstroms (Å).

Discussion

Allosteric modulation of L-malate dehydration activity of AtFUMs gives clues for the network encompassing fumarate accumulation during nitrogen assimilation

In plants, carbon flow through the TCA cycle can follow two different pathways: the catabolic stage, characterized by decarboxylative energy-producing reactions and the anabolic stage, during which carbon is conserved and redirected to the glyoxylate shunt or the amino acid metabolism [15]. Along with MDH, FUM participates in opposite reactions in both of these TCA cycle branches but, unlike MDH, FUM activities are not energy (NAD/NADH)-dependent reactions. Thus, FUM can be subjected to a specific metabolic regulation not described to date.

Here, we present a comprehensive view of the biochemical properties of plant FUM through the characterization of the complete set of *A. thaliana* isoforms. Consistent with their belonging to Class II FUM, the three gene products of *AtFUM1* and *AtFUM2* are homotetrameric proteins and the heterologous expression strategy set here resulted in AtFUM1 and AtFUM2 active enzymes. Unlike *diacylglycerol kinase* [17] and *RuBisCO activase* [18] genes, which generate isoenzymes with modified properties by alternative maturation of the transcripts, one of the proteins encoded by the *AtFUM2* gene (AtFUM2b) lacks any enzymatic activity measured *in vitro*. Further studies are necessary to establish the role of AtFUM2b transcript, such as whether it is translated *in vivo* or it is involved in a mechanism of RNA-based regulation of FUM activity. The complementation of *AtFUM2* knockout mutant plants with AtFUM2 cDNA as a transgene does not fully replicate endogenous gene functions, such as the diurnal fumarate and starch accumulation profiles [11], which is consistent with a regulation of FUM activity at the level of RNA-processing.

For both FH and MD activities, optimum pH of recombinant AtFUM1 and -2 were above the physiological pH values (7.0–7.3) (Table 1). For both enzymes, FH reaction is less affected than MD reaction by changes in pH beyond its optimum value (Fig. 4). Thus, we predict a suboptimal FUM activity in

Arabidopsis cells and a direction of the carbon flow through FUM reaction sensitive to pH changes. In agreement with the thermodynamic direction of the reaction (K_{eq} = [L-malate]/[fumarate] = 4.42 at pH 7.4 and 25 °C; [19], AtFUM1 and -2 favor the L-malate synthesis (FH activity) over the reverse reaction (MD activity) with higher V_{max} values and affinity for its substrate (Table 1). A preference for L-malate synthesis was also described for recombinant *E. coli* FUMC [20] and a purified enzyme from yeast [21], which is coherent with the role of FUM in the TCA cycle. However, *AtFUM2* gene is required for fumarate accumulation in Arabidopsis plants grown on high inorganic N media, suggesting that the encoded protein exhibits a preference for MD activity under certain conditions [11].

In this respect, the effect of metabolic compounds on AtFUM1 and -2 activities strongly suggests that fumarate synthesis could be relevant *in vivo*, as the MD reaction was the most up-regulated one (Table 2). For both enzymes, OAA, Asn, and Gln stimulated the MD activity while inhibited, or did not modify, the FH reaction. Pyruvate also stimulated the synthesis of fumarate in AtFUM1 (Table 2) and, along with α-KG, favored this reaction in AtFUM2 by inhibiting the FH activity (Table 2). Gln and Asn concentrations are in the millimolar order in barley [22], spinach [23], and maize [24] cells. Also, the concentration of organic acids is around 10–20 mM in species such maize, *Sorghum bicolor* and *Brassica napus* [25]. Thus, the $K_{(app)}$ values for organic acids and amino acids of AtFUMs are well within their probable physiological concentration range (Table 2), suggesting that they are important regulators of FUM activity *in vivo*. Furthermore, it is reasonable to expect a dominance of MD reaction over the FH reaction under conditions that favor the accumulation of organic acids and amino acids, as the FH to MD catalytic efficiencies ratio of recombinants AtFUMs was inverted in the presence of OAA, Asn, or Gln (Table 3). Such metabolic condition could take place in plants during the N assimilation (Fig. 7). It has been shown that Gln and Asn are particularly accumulated in Arabidopsis and tobacco plants grown on high N supply [26,27]. Also in these species, nitrate up-regulates the *pepc*, *pyruvate kinase*, *citrate synthase*, and *isocitrate dehydrogenase* genes [28–30]. The increased flux of carbon through these reactions could lead to permanent/transitory accumulation of OAA, pyruvate, and/or α-KG. Thus, when N supply is high, the fumarate synthesis for AtFUMs is preferred over the L-malate synthesis as a consequence of a concerted allosteric modulation exerted by the N-dependent accumulation of organic and amino acids (Fig. 7). Contrary to our observations, the partial purification and characterization of mitochondrial FUM from pea indicated an inhibition of the MD activity by pyruvate and α-KG [31]. Thus, the regulation of FUM activity in Arabidopsis seems to be mainly intended to fumarate accumulation.

It is worth noting that the above results clearly point out the mitochondrial AtFUM1 as coordinately acting with cytosolic AtFUM2 for fumarate accumulation through a reductive branch of the TCA cycle (Fig. 7). This could occur during the day when the N assimilation in leaf is more relevant. However, at night, we predict that the MD reaction of AtFUM1 is deactivated because of a decrease in the Gln levels during this period [22,26,29]. Thus, FH activity can become more relevant and is further stimulated by Glucose 6P (Table 2) derived from starch breakdown. This integrated regulation of AtFUM1 would serve for the mobilization of the stored fumarate and would also ensure the carbon flux through glycolysis and TCA cycle under the heterotrophic growth phase. Cytosolic AtFUM2 could also be involved in fumarate mobilization at night. The recombinant isoform exhibits the highest fumarate affinity (Table 1) and the MD activity of AtFUM2 would also be deactivated by the decreased levels of Gln during the night. In addition, since fumarate is mainly accumulated in the cytosol, the mass action ratio of the FUM reaction is far from equilibrium during the night [11]. Finally, although *AtFUM2* knockout mutant plants accumulate very low fumarate, the levels of this acid at night are similar to those measured in the daylight [11], suggesting that AtFUM2 is responsible for both fumarate accumulation and its mobilization.

Disulfide bridge formation of AtFUM1 and AtFUM2 may be involved in the redirection of the carbon flux under oxidative stress

Arabidopsis FUM1 has been identified as a thioredoxin target *in vitro* [32,33] but the functional role of this interaction has not been investigated. In the present work, we provide evidence that the FUM activity is modulated by the redox status in plants. DAA-oxAtFUMs form high mass molecular aggregates (Fig. 3A) and exhibit inhibited FH and MD activities either in their native or recombinant forms (Fig. 5) as a consequence of a decrease in both the affinity for the substrates and the maximum catalytic activity (Table 3). The biochemical properties of oxAtFUMs were completely reversed by Arabidopsis leaf extracts with added NADPH (Fig. 3C), indicating that their reduction can be accomplished *in vivo*. By applying LC–MS-based method, it was proved that, under mild

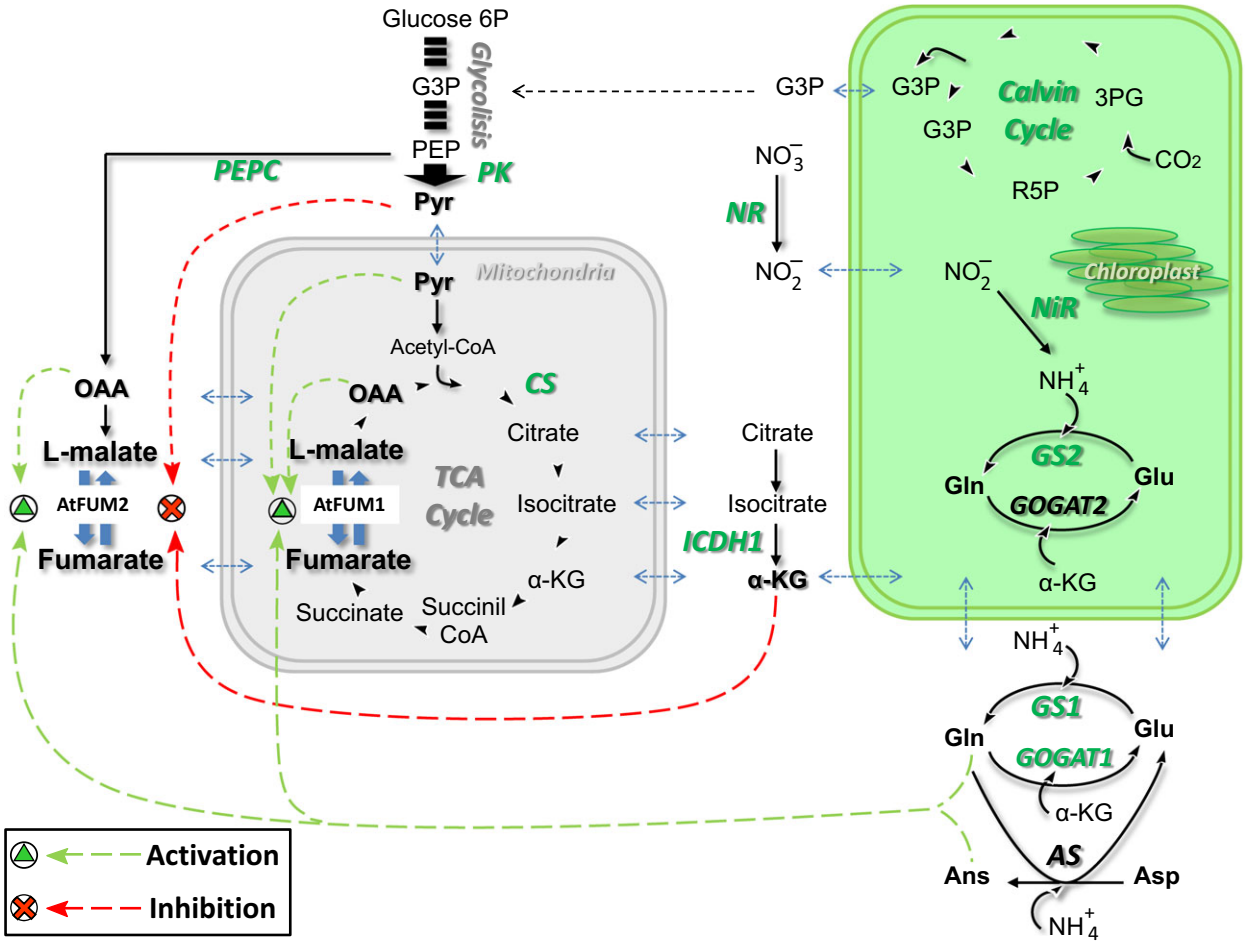

Fig. 7. A model for allosteric regulation of AtFUM1 and 2 during nitrogen assimilation in *A. thaliana*. The coordinate regulation of AtFUMs by allosteric effectors, particularly Gln, Asn, OAA, Pyr, and α-KG, provides a mechanism for the control of cytosolic and mitochondrial acid organic flux for fumarate accumulation during N assimilation, as discussed in the text. Enzymatic paths that are up-regulated by nitrate are shown in green-shaded letters. Double-dotted arrows indicate metabolite transport between compartments. PEPC, phosphoenolpyruvate carboxylase; PK, pyruvate kinase; CS, citrate synthase; ICDH1, cytosolic (NADP-dependent) isocitrate dehydrogenase; NR, nitrate reductase; NiR, nitrite reductase; GS1 and GS2, cytosolic and plastidial Gln synthetase, respectively; GOGAT1 and GOGAT2, cytosolic (NADP-dependent) and plastidial (Fd-dependent) Gln α-ketoglutarate aminotransferase, respectively; α-KG, α-ketoglutarate; PEP, phosphoenolpyruvate; Pyr, pyruvate; G3P, glyceraldehyde 3-phosphate; 3PG, 3-phosphoglycerate; R5P, ribulose 5-phosphate.

oxidant conditions, AtFUM2 presents a Cys339-Cys339 intermolecular disulfide bridge (Table S3). Homologous residue to Cys339 in AtFUM2 is present as Cys306 in AtFUM1, thus the same covalent modification could be expected for the mitochondrial enzyme. As the search performed in the MS analysis was targeted, it cannot be excluded that additional disulfide bridges could affect the kinetic parameters of AtFUMs. However, the physiological relevance of a disulfide bridged involving Cys339 (Cys306 in AtFUM1) should be noted. This residue is located at the beginning of the 'SS loop' that is part of the active site (Fig. 6). It is well-known that, in the aspartase/fumarase superfamily, binding of the substrate induces a conformational change in the 'SS loop' from an open to a closed conformation in which the loop moves over the active site [6]. Thus, we predict that a Cys339-Cys339 (and probably Cys306-Cys306 in AtFUM1) intermolecular disulfide bridge links two 'SS loops', restricting their flexibility and affecting the catalysis of two adjacent active sites (Fig. 6). The significantly lower catalytic efficiency values of oxiAtFUM1 and -2 support this hypothesis (Table 3).

In proteins, redox-sensitive cysteines are recognized as a signaling mechanism, promoting conformational changes that modulate biological activity and influence protein–protein interactions or subcellular localization [34,35]. In the case of AtFUM1, FH and MD activities

were dramatically inhibited by oxidation (Table 3). This could constitute an additional restriction on the flux of carbon through FUM reaction in the TCA cycle beyond the decreased AtFUM1 protein abundance [36] and the repressed *AtFUM1* gene activity by oxidative stress [37]. In plants, the citrate synthase [38], aconitase [39], and 2-oxogutarate dehydrogenase [40] are also sensitive to oxidative inactivation. The overall suppression of the TCA cycle is part of a general mechanism of redirection of carbon from respiration into the oxidative pentose phosphate pathway for NADPH production [37]. Interestingly, the MD reaction of AtFUM2 was comparatively much less affected by oxidation (Table 3). Thus, a significant fumarate synthesis driven by AtFUM2 can be expected, even under conditions that increase reactive oxygen species (ROS). Moreover, it remains to be analyzed if AtFUM2 is able to move to the nucleus under oxidative conditions, as its animal and yeast cytosolic counterparts do [7]. If so, fumarate accumulation in this compartment of plants could also be associated to the signaling pathways that lead to double-stranded break repairs following DNA damage by ROS [7].

Overall, the allosteric and covalent regulatory pattern of Arabidopsis FUMs strongly point out to a tight regulation of the C4-organic acids metabolism in plants. The estimated flux control coefficients of dark respiration for the eight TCA enzymes support this notion, as much of the control through the pathway is mainly divided between FUM and MDH [41]. Finally, it will be a challenge for future studies to evaluate our regulatory framework over the dynamic association of AtFUMs into the TCA cycle metabolon. Isotope dilution experiments indicated fumarate channeling between FUM1 and MDH2 in plant mitochondria, providing *in vivo* evidence of protein–protein interactions [42]. However, fumarate levels exhibit a diurnal profile of synthesis/consumption, which requires the dissociation of the metabolon at some point in the photoperiod. Hence, allosteric and covalent regulation of FUMs could integrate environmental signals regulating the dynamics of TCA metabolon formation and altering the carbon flux through anabolic/catabolic branches of TCA cycle.

Cytosolic FUM2 could be present in other plant species as a prerequisite for fumarate accumulation

In *A. thaliana*, the presence of FUM in the cytosol is under the control of a different gene from that encoding the mitochondrial isoform [11]. This phenotypic trait could be not exclusive of *A. thaliana*, as FUM phylogenetic tree of plants shows genes encoding for putative cytosolic isoforms (*FUM2*) in several species (Fig. 2). Moreover, our results suggest that FUM2 evolved independently in many of these species, as it is present as a paralogous gene in unrelated species. Similar observations were recently described from the phylogenetic patterns based on the amino acid sequences of FUM [43], supporting that the evolutionary history for a cytosolic-specific FUM2 isoform in plants has been drawn by a process of parallel evolution.

In the Brassicaceae family, tree topology is consistent with an origin of *FUM2* before the Arabidopsis (Linage I) and Brassica (Lineage II) split followed by a biased loss of *FUM2* in several members, probably as a consequence of the substantial genome fractionation that characterized crucifers' evolution [44]. In this regard, the Brassicaceae evolutionary history has been characterized by accelerated speciation rates, which are the highest among those reported for land plants to date [45]. Despite the fact that gene duplication has constituted the raw material for the adaptive evolution of new species, the processes by which duplicated genes become fixed in the genome were based on their ability to acquire either subfunctionalization or neofunctionalization [46]. Recently, Dyson *et al.* [47] have provided compelling evidence that *AtFUM2* is essential for *A. thaliana* acclimation to low temperatures. Moreover, biomass production at low temperatures exhibits a surprisingly high positive correlation with AtFUM2 transcript and fumarate levels [48]. In addition, Riewe *et al.* [49] carried out a comparative analysis of the geographical distribution of a large population of a natural knockdown mutant *AtFUM2* of *A. thaliana* (the C24 allele), which is common in Europe. They found that, while Col-0 plants can be found in the North/East, C24 variants are restricted to South/West Europe. This distinct geographical distribution pattern of naturally occurring genetic variant would be warning that *AtFUM2* confers certain competitive advantages under cold environmental conditions. Given that data at hand, and taking into account that the formation of current species within the major Brassicaceae lineages started with the onset of the last glaciation period [45], it is feasible to suppose that the pre-*FUM2* gene was fixed in the *A. thaliana* recent ancestor by a neofunctionalization related to cold adaptation.

The association between a gene encoding for cytosolic FUM and the accumulation of large amounts of fumarate has only been studied in *A. thaliana* to date. However, *in silico* analysis suggests that it could be extensible to other species. In Brassicaceae, *B. strica* (rock cress) accumulates fumarate at levels that are comparable to those found in *A. thaliana* [13] and has

two putative functional *FUM2* genes (Fig. 2). Outside crucifer family, *Phaseolus vulgaris* (bean) and *Glycine max* (soybean) exhibit moderately high levels of this acid [13] and they would both express at least one FUM2 (Fig. 2). Thus, a specific gene for cytosolic FUM might be a prerequisite for the fumarate accumulation in plants. It would be interesting to examine this hypothesis by searching for a *FUM2* gene in other species showing high fumarate levels, such as *Arabidopsis griffithiana*, *Arabidopsis himalaica, Alecea rosea*, or *Fumaria officinalis*, from which fumaric acid was first isolated and named [13]. However, it may also be possible that plant species without a *FUM2* gene might even possess FUM activity in the cytosol because mitochondrial FUM1 could display a dual localization, as was observed for homologous FUM from animals and yeast [7]. In this sense, FUM was found in the extracellular space in carrot suspension cells grown on L-malate [50]. However, a specific gene encoding the cytosolic FUM offers a finer-tuning mechanism of regulation of FUM activity than that supported by a single promoter. At least in *A. thaliana*, this has provided an adaptive advantage allowing fumarate to accumulate in leaves to be used as a flexible and transportable carbon sink [13] for the rapid growth when nitrogen becomes available [11,29] and to acclimate photosynthesis to low temperatures [47,48].

Experimental procedures

Retrieval of sequences and alignments

Coding sequences of human and yeast FUM were recovered from the National Center for Biotechnology Information database (http://ncbi.nlm.nih.gov). For plants and algal species with entire genome information, sequences were extracted from www.phytozome.net, while some Brassicaceae FUMs were retrieved from Brassica Database (http://brassicadb.org/brad/index.php). Accession numbers of FUM sequences used in the present study is provided in Table S4. For amino acidic comparisons and general editing, the sequences were aligned in a ClustalW format.

Prediction for translation initiation sites (TIS) and subcellular localization of proteins

In order to identify alternative TIS located upstream or downstream of the annotated start codon, the 5′ untranslated region (5′ UTR) for each *FUM* gene were analyzed by using NetStart 1.0 Prediction Server [51].

Protein localization was analyzed using MitoProt II [52], TargetP 1.1 [53], and SignalP 4.0 [54] using default program parameter settings. Sequences were considered as localized in the predicted subcellular compartment when the three programs generated matching results.

Phylogenetic and molecular evolutionary data analyses

For phylogenetic tree construction, FUM coding sequences were translated into amino acids and a multiple alignment was constructed with MUSCLE (Multiple Sequence Comparison by Log-Expectation; [55]). Once translated back into nucleotides, the alignment was manually edited for missing gaps or poorly aligned regions. The final FUM alignment consisted of 87 coding sequences and 1427 characters. The phylogenetic tree was inferred by Bayesian inference (BI) methods via the MRBAYES 3.1.2 software [56]. The best-fit model was the GTR substitution model with a gamma shape parameter and a proportion of invariant sites (GTR + G + I) as determined through hierarchical likelihood ratio tests.

In BI analysis, two parallel runs, each including four Metropolis-coupled Markov chain Monte Carlo (MC3) analysis, were run for 2 000 000 generations and sampled every 500 generations for each partition scheme. An incremental heating scheme of three heated chains and one cold chain in each run was used, with a temperature parameter setting of 0.08. In order to confirm that the chains achieved stationary, 'burn-in' plots were evaluated by plotting log likelihood against generation number. Also, the final average standard deviation of split frequencies was used as the convergence index, in which values < 0.01 indicated good convergence. Clade convergence posterior probabilities within and between runs were checked using the Potential Scale Reduction Factor (PSRF). After determining convergence, the initial 25% of the sampled trees for each MC3 run was discarded as burn-in, and the post burn-in trees were used to generate a 50% majority-rule consensus tree. The percentage of samples recovering any particular clade in a BI analysis represents such posterior probability (BPP) of a clade. Nodes with BPP values $\geq 95\%$ were considered highly supported and $\leq 95\%$ not supported. The resulting tree was displayed using the FIGTREE v1.4 software (http://tree.bio.ed.ac.uk/software/figtree) and visually edited. Substitutions per site are denoted as a separate bar with a number in the phylogenetic tree.

Analysis for putative paralogous *FUMs* was conducted using the criteria established for the identification of young duplicate genes [57]. We calculated the rate of synonymous substitutions (K_s) for *FUM1* and *FUM2* gene pairs and considered *FUM2* as a paralogous gene if $K_s \leq 0.283$. Because K_s is not under selective pressure, its value is an estimative measurement of time divergence among sequences. K_s value of 0.283 was calculated from the mean K_s value of 10 single (low)-copy orthologous genes that were described as evolutionary distant markers among species [58,59]. K_s value for the aligned gene pairs was

calculated using MEGA version 6 [60]. Analyses were conducted using the Nei–Gojobori model with all positions containing gaps and missing data eliminated.

Cloning of AtFUM cDNAs

Total RNA from Arabidopsis leaf was isolated from 100 mg of tissue using the TRIzol reagent (Gibco-BRL, Thermo Fisher Scientific, Waltham, MA, USA). RNA was converted into first-strand cDNA using SuperScript II reverse transcriptase (Invitrogen, Carlsbad, CA, USA). Full-length cDNAs were amplified using platinum Pfx DNA polymerase (Invitrogen) and specific primers. Oligonucleotide primers were designed to introduce unique BamHI and SalI sites at the 5′ and 3′ends, respectively. In order to express the mature AtFUM1, a specific primer containing the first codon downstream of the predicted targeting peptide cleavage site was generated. To amplify AtFUM1 and the different versions of AtFUM2, the following primer combinations were used:

Fum1for: GGATCCATGTATTCGACCTCGTTTA
Fum1rev: GTCGACTCAATCGGAGGGACCAATCA
Fum2(2b)for: GGATCCATGGCCGCTTTGACAATGCA
Fum2rev: GTCGACTTAAATCCAAAATAGAACAA
Fum2brev: TTTTTATTTGTTGTTCTGTGTCAGA
Fum2bdel: GTCGGACTTATTTAATGTGCATCCTTCTTT

The PCR products were cloned into pGEM-TEasy (Promega, Promega Corporation, Madison, WI, USA) and completely sequenced.

Heterologous expression and purification of recombinant AtFUMs

For the expression of the mature AtFUM1 and the different forms of AtFUM2, the cDNA fragment encoding each protein was subcloned in the pET32a vector, which generates N-terminal His-tag fusion proteins, using the BamHI and SalI sites. BL21(DE3) *E. coli* cells were transformed with pET32-AtFUM1, pET32-AtFUM2, pET32-AtFUM2b and pET32-AtFUM2bdel. The cells containing the vectors were selected on LB-agar plates supplemented with 100 $\mu g \cdot mL^{-1}$ ampicillin. The transformed cells were grown in LB medium plus 100 $\mu g \cdot mL^{-1}$ ampicillin until the culture reached an $A_{600\ nm}$ of 0.6. The inductor lactose (1% w/v) was added, and the cells were cultured for a further 16 h at 16 °C. The cells were then harvested by centrifugation for 5 min at 4000 ***g***; resuspended in a buffer containing 50 mM Tris/HCl (pH 8), 0.25 M NaCl, 0.1% triton X-100, and 1 mM phenyl methyl sulfonide fluoride (PMSF); sonicated and centrifuged for 10 min at 7000 ***g*** at 4 °C. The supernatant (soluble fraction) was used for protein purification onto a Niquel-NTA column according to the protocol provided by the manufacturer (Novagen, Merck, Darmstadt, Germany) but using 200 mM imidazole and 0.5 M NaCl for elution.

The enzymes were then concentrated on Centricon YM-50 (Amicon) and desalted using a buffer A (50 mM Tris/HCl pH 8, 4 mM 1,4-dithiothreitol (DTT), and 1 mM PMSF). Purified fusion AtFUM proteins were then incubated with thrombin endoprotease (1 : 100) for 2 h at 15 °C to remove the N terminus encoded by the expression vector. The proteins were further purified by using a gel-filtration chromatography on a ÄKTA purifier system (GE Healthcare, Chicago, IL, USA) using a Biosep-SEC-S3000 column (Phenomenex, Torrance, CA, USA) equilibrated with buffer A, divided into aliquots and stored at −80 °C with 50% glycerol for further studies. The typical protein yield of AtFUMs was nearly 1 mg/100 mL of bacterial culture. Protein concentration was determined by the BioRad Protein Assay with total serum protein as standard.

Protein crude extract preparations

Arabidopsis leaves of 5-week-old plants were ground in N_2, and the resulting powder was suspended in a buffer containing 100 mM Tris/HCl (pH 7), 2 mM $MgCl_2$, 1 mM EDTA, 0.05% Triton X-100, and 20% glycerol. Then, 10 μL inhibitors cocktail (Thermo Scientific) was added to 1 mL of buffer. The homogenates were clarified by centrifugation. The supernatants were desalted using a Sephadex G-50 column equilibrated with buffer 100 mM Tris/HCl (pH 7), 2 mM $MgCl_2$, and 20% glycerol and separated for activity measurements or subjected to electrophoresis.

Enzymatic activity measurement

Fumarate hydratase and MD activities of purified recombinant AtFUMs were measured spectrophotometrically at 240 nm. The enzymatic reactions were performed in quark cuvettes in a final volume of 0.5 mL of equilibrated buffer. The reaction was started by the addition of fumarate or L-malate. An experimentally determined $\varepsilon_{240\ nm}$ of 2.34 $mM^{-1} \cdot cm^{-1}$ was used in the calculation of the activity. One unit of fumarase activity was defined as 1 μmol of L-malate (FH reaction) or fumarate (MD reaction) generated per minute. Alternatively, the FH activity of desalted Arabidopsis leaf crude extracts was measured through the fumarase and NADP-malic enzyme (NADP-ME) coupled assay. In this case, the standard reaction mixture contained buffer A plus 2 mM $MgCl_2$, 0.5 mM NADP, and 70 μg of recombinant purified C_4-NADP-ME of maize [61] in a final volume of 0.5 mL. The reaction was started by the addition of fumarate and the activity was registered spectrophotometrically at 340 nm for the NADPH formation ($\varepsilon_{340\ nm} = 6.22\ mM^{-1} \cdot cm^{-1}$).

Initial velocity studies were performed by varying the concentration of substrate around its K_m value. All kinetic parameters were calculated at least in triplicate and adjusted to nonlinear regression using SIGMA PLOT 12.0 program (Systat Software, Inc., San Jose, CA, USA). All activity assays were carried out at 30 °C in a Jasco V630 spectrophotometer.

Protein concentration was determined by the BioRad Protein Assay with total serum protein as standard.

The profiles of activity versus pH were determined using the standard assay method at nonsaturating levels of substrates (0.3 mM fumarate or 3.0 mM L-malate). The enzyme activity was assayed over the pH range 5.0–5.6 in 50 mM acetic acid/Na acetate buffer; 5.6–6.8 in 50 mM MES-NaOH buffer; 6.8–7.3 in 50 mM MOPS-KOH buffer; and 7.3–8.9 in 50 mM Tris/HCl buffer. All the experiments were performed in triplicate.

When testing different compounds as possible inhibitors or activators of the enzymatic activity, FUM activity was measured in the presence of different concentrations of each effector and nonsaturating concentrations of substrate ($K_m/3$). The enzymes were preincubated with each compound and the reactions were started by the addition of the substrate. $Ka_{(app)}$ (as A_{50}) or $Ki_{(app)}$ (as I_{50}) value for each modulator was obtained by nonlinear regression of % activity versus effector concentration curves. When OAA was evaluated as effector, the determinations were corrected for the tautomerization of OAA [62].

Gel electrophoresis

SDS/PAGE was performed in 10% (w/v) polyacrylamide gels according to Laemmly [63] without addition of 2-mercaptoethanol to the Sample Buffer. Native PAGE was performed using a 6% (w/v) acrylamide separating gel. Electrophoresis was run at 12 V at 10 °C. Gels were visualized with Coomassie Blue or, alternatively for native electrophoresis, gels were assayed by fumarase activity by incubation with a solution containing 50 mM Tris/HCl pH 8, 20 mM fumarate, 0.8 mM $NADP^+$, 2 mM $MgCl_2$, 100 μg of recombinant purified C_4-NADP-ME of maize, 35 $\mu g \cdot mL^{-1}$ nitroblue tetrazolium, and 0.85 $mg \cdot mL^{-1}$ phenazine methosulfate at 30 °C.

Gel-filtration chromatography

Molecular masses of recombinant FUM1, FUM2, and FUM2b were evaluated by gel-filtration chromatography on an ÄKTA purifier system (GE Healthcare) using a Biosep-SEC-S3000 column (Phenomenex). The column was equilibrated with 20 mM Tris/HCl at pH 8.0 in the presence or absence of 100 mM NaCl and calibrated using molecular mass standards (Sigma-Aldrich, Merck, Darmstadt, Germany). The samples and the standards were applied in a final volume of 100 μL at a constant flow rate of 0.5 $mL \cdot min^{-1}$. All the experiments were performed in triplicate.

Redox modulation of the AtFUMs activities

The purified recombinant AtFUMs (100 μg) and Arabidopsis leaf crude extracts (50 μg of total protein) were incubated at 0 °C with different concentrations of DAA (oxidizing agent) or DTT (reducing agent). At different incubation times, aliquots were withdrawn and assayed for fumarase activity. Modification of the recombinant enzymes was stopped by dilution (at least 100-fold) of redox compounds in the assay medium. No significant decrease in activity was found when the recombinant AtFUMs or crude extracts were incubated up to 2 h in the absence of redox compounds. Addition of these compounds (diluted 100-fold) to the assay medium had no significant effect on the enzyme activity assay. The determination of the kinetic parameters of AtFUM1 and -2 incubated with 2 mM DAA for 90 min at 0 °C (oxAtFUM) was performed as previously described.

The reduction of oxAtFUMs was also tested using Arabidopsis crude extracts. For this, the oxAtFUM1 fusion protein (His-Tag·oxAtFUM1) was linked to NTA-Ni chromatographic matrix and incubated with desalted crude Arabidopsis leaf extracts, in the presence or the absence of 100 μM NADPH, for 1 h at 15 °C. After that time, several washes of the matrix were performed to remove extract components and the bound recombinant protein was eluted with 200 mM imidazole and analyzed by Coomassie-stained SDS/PAGE under nonreduction conditions.

Mass spectrometry and data analysis

Approximately 10 μg of reduced (DTT-treated) or oxidized (DAA-treated) AtFUM2 were run on an 8% (w/v) polyacrylamide SDS/PAGE in the absence of any reductant. Coomassie colloidal-stained bands were excised from the gel and treated with 55 mM iodoacetamide, a sulfhydryl-reactive alkylating reagent used to block reduced cysteine by carbamidomethylation. Protein digestion and MS analysis were performed at the Proteomics Core Facility CEQUIBIEM, at the University of Buenos Aires/CONICET (National Research Council) as follows: excised protein bands were sequentially washed with 50 mM ammonium bicarbonate, 25 mM ammonium bicarbonate 50% acetonitrile, and 100% acetonitrile; and in-gel digested with 100 ng of trypsin in 25 mM ammonium bicarbonate overnight at 37 °C. Peptides were recovered by elution with 50% acetonitrile–0.5% trifluroacetic acid, including brief sonication, and further concentrated by speed-vacuum drying. Samples were resuspended in 15 μL of water containing 0.1% formic acid and desalted using C18 zip tips (Merck Millipore) and eluted in 10 μL of H20 : ACN : FA 40 : 60 : 0.1%.

Full-scan mass spectra were acquired in the Orbitrap analyzer. The scanned mass range was 400–1800 m/z, at a resolution of 70 000 at 400 m/z and the 12 most intense ions were sequentially isolated, fragmented by HCD, and measured in the Orbitrap analyzer. Peptides with a charge of +1 or with unassigned charge state were excluded from fragmentation for MS2. Q Exactive raw data were processed using

PROTEOME DISCOVERER software (version 1.4; Thermo Scientific) and searched against Fumarase sequences obtained from The Arabidopsis Information Resource protein database (buildTAIR10_pep_20101214, ftp://ftp.Arabidopsis.org/home/tair/Proteins/TAIR10_protein_lists/) with trypsin specificity and a maximum of two missed cleavages at a protein. Carbamidomethylation of cysteine residues and oxidation of methionine were set as variable modifications.

For the analysis of linked disulfides in oxidized AtFUM2, the masses of the dipeptides were calculated using PROTEIN PROSPECTOR software. Masses of doubly, triply, or quadruply charged ions corresponding to theoretical dipeptide masses for possible linked peptides involving Cys339 (Table S4C) were compared manually with the peaklists obtained. The MS2 spectra of the matching peaks were analyzed and compared with theoretical fragmentation patterns, in order to verify the amino acid sequence of the dipeptides.

Structure model of AtFUM2

For the modeling of Arabidopsis FUM2 structure, the Swiss PDB Viewer was used. The amino acid sequence of AtFUM2 was fitted to the crystal structure of fumarase from yeast (PDB ID: 1YFM). Modifications of the structure were made with the Discovery Studio Visualizer v16.1.015350.

Acknowledgements

We thank the staff of the English Department (Facultad de Ciencias Bioquímicas y Farmacéuticas - UNR) for the language correction of the manuscript. MAT, MPV, SM, CSA, and MFD are members of the Researcher Career of the National Council of Scientific and Technical Research (CONICET). JPZ is a research fellow at the same institution. This work has been financially supported by the National Agency for Scientific and Technological Promotion and CONICET.

Author contribution

MAT, MFD, and CSA developed the concept and designed the experiments of this study. JPZ prepared recombinant proteins and was involved in biochemical data acquisition. MAT performed the phylogenetic analyses. SM and MPV were specifically involved in the collection and interpretation of MS data. MAT, in collaboration with the other authors, drafted the manuscript.

References

1 Tseng CP, Yu CC, Lin HH, Chang CY & Kuo JT (2001) Oxygen- and growth rate-dependent regulation of *Escherichia coli* fumarase (FumA, FumB, and FumC) activity. *J Bacteriol* **183**, 461–467.

2 Woods SA, Miles JS, Roberts RE & Guest JR (1986) Structural and functional relationships between fumarase and aspartase. Nucleotide sequences of the fumarase (fumC) and aspartase (aspA) genes of *Escherichia coli* K12. *Biochem J* **237**, 547–557.

3 Weaver TM, Levitt DG, Donnelly MI, Stevens PP & Banaszak LJ (1995) The multisubunit active site of fumarase C from *Escherichia coli*. *Nat Struct Biol* **2**, 654–662.

4 Weaver T, Lees M, Zaitsev V, Zaitseva I, Duke E, Lindley P, McSweeny S, Svensson A, Keruchenko J, Keruchenko I *et al.* (1998) Crystal structures of native and recombinant yeast fumarase. *J Mol Biol* **280**, 431–442.

5 Picaud S, Kavanagh KL, Yue WW, Lee WH, Muller-Knapp S, Gileadi O, Sacchettini J & Oppermann U (2011) Structural basis of fumarate hydratase deficiency. *J Inherit Metab Dis* **34**, 671–676.

6 Puthan Veetil V, Fibriansah G, Raj H, Thunnissen AMWH & Poelarends GJ (2012) Aspartase/fumarase superfamily: a common catalytic strategy involving general base-catalyzed formation of a highly stabilized aci-carboxylate intermediate. *Biochemistry* **51**, 4237–4243.

7 Yogev O, Naamati A & Pines O (2011) Fumarase: a paradigm of dual targeting and dual localized functions. *FEBS J* **278**, 4230–4242.

8 Suzuki T, Yoshida T & Tuboi S (1992) Evidence that rat liver mitochondrial and cytosolic fumarases are synthesized from one species of mRNA by alternative translational initiation at two in-phase AUG codons. *Eur J Biochem* **207**, 767–772.

9 Sass E, Blachinsky E, Karniely S & Pines O (2001) Mitochondrial and cytosolic isoforms of yeast fumarase are derivatives of a single translation product and have identical amino termini. *J Biol Chem* **276**, 46111–46117.

10 Yogev O, Yogev O, Singer E, Shaulian E, Goldberg M, Fox TD & Pines O (2010) Fumarase: a mitochondrial metabolic enzyme and a cytosolic/nuclear component of the DNA damage response. *PLoS Biol* **8**, e1000328.

11 Pracharoenwattana I, Zhou W, Keech O, Francisco PB, Udomchalothorn T, Tschoep H, Stitt M, Gibon Y & Smith SM (2010) Arabidopsis has a cytosolic fumarase required for the massive allocation of photosynthate into fumaric acid and for rapid plant growth on high nitrogen. *Plant J* **62**, 785–795.

12 Araújo WL, Nunes-Nesi A & Fernie AR (2011) Fumarate: multiple functions of a simple metabolite. *Phytochemistry* **72**, 838–843.

13 Chia DW, Yoder TJ, Reiter WD & Gibson SI (2000) Fumaric acid: an overlooked form of fixed carbon in

Arabidopsis and other plant species. *Planta* **211**, 743–751.
14 Lee CP, Eubel H & Millar AH (2010) Diurnal changes in mitochondrial function reveal daily optimization of light and dark respiratory metabolism in Arabidopsis. *Mol Cell Proteomics* **9**, 2125–2139.
15 Sweetlove LJ, Beard KF, Nunes-Nesi A, Fernie AR & Ratcliffe RG (2010) Not just a circle: flux modes in the plant TCA cycle. *Trends Plant Sci* **15**, 462–470.
16 Kosower NS & Kosower EM (1987) Formation of disulfides with diamide. *Methods Enzymol* **143**, 264–270.
17 Snedden WA & Blumwald E (2000) Alternative splicing of a novel diacylglycerol kinase in tomato leads to a calmodulin-binding isoform. *Plant J* **24**, 317–326.
18 Werneke JM, Chatfield JM & Ogren WL (1989) Alternative mRNA splicing generates the two ribulosebisphosphate carboxylase/oxygenase activase polypeptides in spinach and Arabidopsis. *Plant Cell* **1**, 815–825.
19 Krebs HA (1953) The equilibrium constants of the fumarase and aconitase systems. *Biochem J* **54**, 78–82.
20 Estévez M, Skarda J, Spencer J, Banaszak L & Weaver TM (2002) X-ray crystallographic and kinetic correlation of a clinically observed human fumarase mutation. *Protein Sci* **11**, 1552–1557.
21 Pines O, Even-Ram S, Elnathan N, Battat E, Aharonov O, Gibson D & Goldberg I (1996) The cytosolic pathway of L-malic acid synthesis in *Saccharomyces cerevisiae*: the role of fumarase. *Appl Microbiol Biotechnol* **46**, 393–399.
22 Winter H, Robinson D & Heldt H (1993) Subcellular volumes and metabolite concentrations in barley leaves. *Planta* **191**, 180–190.
23 Winter H, Robinson DG & Heldt HW (1994) Subcellular volumes and metabolite concentrations in spinach leaves. *Planta* **193**, 530–535.
24 Weiner H & Heldt H (1992) Inter- and intracellular distribution of amino acids and other metabolites in maize (*Zea mays* L.) leaves. *Planta* **187**, 242–246.
25 Jones DL (1998) Organic acids in the rhizosphere – a critical review. *Plant Soil* **205**, 25–44.
26 Scheible WR, Krapp A & Stitt M (2000) Reciprocal diurnal changes of phosphoenolpyruvate carboxylase expression and cytosolic pyruvate kinase, citrate synthase and NADP-isocitrate dehydrogenase expression regulate organic acid metabolism during nitrate assimilation in tobacco leaves. *Plant Cell Environ* **23**, 1155–1167.
27 Igarashi D, Tsuchida H, Miyao M & Ohsumi C (2006) Glutamate: glyoxylate aminotransferase modulates amino acid content during photorespiration. *Plant Physiol* **142**, 901–910.
28 Scheible WR, Gonzalez-Fontes A, Lauerer M, Muller-Rober B, Caboche M & Stitt M (1997) Nitrate acts as a signal to induce organic acid metabolism and repress starch metabolism in tobacco. *Plant Cell* **9**, 783–798.
29 Tschoep H, Gibon Y, Carillo P, Armengaud P, Szecowka M, Nunes-Nesi A, Fernie AR, Koehl K & Stitt M (2009) Adjustment of growth and central metabolism to a mild but sustained nitrogen-limitation in Arabidopsis. *Plant Cell Environ* **32**, 300–318.
30 Wang R, Guegler K, LaBrie ST & Crawford NM (2000) Genomic analysis of a nutrient response in Arabidopsis reveals diverse expression patterns and novel metabolic and potential regulatory genes induced by nitrate. *Plant Cell* **12**, 1491–1509.
31 Behal RH & Oliver DJ (1997) Biochemical and molecular characterization of fumarase from plants: purification and characterization of the enzyme–cloning, sequencing, and expression of the gene. *Arch Biochem Biophys* **348**, 65–74.
32 Yoshida K, Noguchi K, Motohashi K & Hisabori T (2013) Systematic exploration of thioredoxin target proteins in plant mitochondria. *Plant Cell Physiol* **54**, 875–892.
33 Daloso DM, Müller K, Obata T, Florian A, Tohge T, Bottcher A, Riondet C, Bariat L, Carrari F, Nunes-Nesi A *et al.* (2015) Thioredoxin, a master regulator of the tricarboxylic acid cycle in plant mitochondria. *Proc Natl Acad Sci U S A* **112**, E1392–E1400.
34 Chi YH, Paeng SK, Kim MJ, Hwang GY, Melencion SMB, Oh HT & Lee SY (2013) Redox-dependent functional switching of plant proteins accompanying with their structural changes. *Front Plant Sci* **4**, 277.
35 Couturier J, Chibani K, Jacquot J-P & Rouhier N (2013) Cysteine-based redox regulation and signaling in plants. *Front Plant Sci* **4**, 105.
36 Sweetlove LJ, Heazlewood JL, Herald V, Holtzapffel R, Day DA, Leaver CJ & Millar AH (2002) The impact of oxidative stress on Arabidopsis mitochondria. *Plant J* **32**, 891–904.
37 Baxter CJ, Redestig H, Schauer N, Repsilber D, Patil KR, Nielsen J, Selbig J, Liu J, Fernie AR & Sweetlove LJ (2007) The metabolic response of heterotrophic Arabidopsis cells to oxidative stress. *Plant Physiol* **143**, 312–325.
38 Schmidtmann E, König A-C, Orwat A, Leister D, Hartl M & Finkemeier I (2014) Redox regulation of Arabidopsis mitochondrial citrate synthase. *Mol Plant* **7**, 156–169.
39 Verniquet F, Gaillard J, Neuburger M & Douce R (1991) Rapid inactivation of plant aconitase by hydrogen peroxide. *Biochem J*, **276**, 643–648.
40 Tretter L & Adam-Vizi V (2000) Inhibition of Krebs cycle enzymes by hydrogen peroxide: a key role of [alpha]-ketoglutarate dehydrogenase in limiting NADH production under oxidative stress. *J Neurosci* **20**, 8972–8979.

41 Araujo WL, Nunes-Nesi A, Nikoloski Z, Sweetlove LJ & Fernie AR (2012) Metabolic control and regulation of the tricarboxylic acid cycle in photosynthetic and heterotrophic plant tissues. *Plant Cell Environ* **35**, 1–21.
42 Zhang Y, Beard KFM, Swart C, Bergmann S, Krahnert I, Nikoloski Z, Graf A, Ratcliffe RG, Sweetlove LJ, Fernie AR *et al.* (2017) Protein-protein interactions and metabolite channelling in the plant tricarboxylic acid cycle. *Nat Commun* **8**, 15212.
43 Cavalcanti JH, Esteves-Ferreira AA, Quinhones CG, Pereira-Lima IA, Nunes-Nesi A, Fernie AR & Araujo WL (2014) Evolution and functional implications of the tricarboxylic acid cycle as revealed by phylogenetic analysis. *Genome Biol Evol* **6**, 2830–2848.
44 Murat F, Louis A, Maumus F, Armero A, Cooke R, Quesneville H, Crollius HR & Salse J (2015) Understanding Brassicaceae evolution through ancestral genome reconstruction. *Genome Biol* **16**, 262.
45 Kagale S, Robinson SJ, Nixon J, Xiao R, Huebert T, Condie J, Kessler D, Clarke WE, Edger PP, Links MG *et al.* (2014) Polyploid evolution of the Brassicaceae during the Cenozoic era. *Plant Cell* **26**, 2777–2791.
46 Wang J, Marowsky NC & Fan C (2013) Divergent evolutionary and expression patterns between lineage specific new duplicate genes and their parental paralogs in *Arabidopsis thaliana*. *PLoS One* **8**, e72362.
47 Dyson BC, Miller MAE, Feil R, Rattray N, Bowsher C, Goodacre R, Lunn JE & Johnson GN (2016) FUM2, a cytosolic fumarase, is essential for acclimation to low temperature in *Arabidopsis thaliana*. *Plant Physiol* **172**, 118–127.
48 Scott IM, Ward JL, Miller SJ & Beale MH (2014) Opposite variations in fumarate and malate dominate metabolic phenotypes of Arabidopsis salicylate mutants with abnormal biomass under chilling. *Physiol Plant* **152**, 660–674.
49 Riewe D, Jeon HJ, Lisec J, Heuermann MC, Schmeichel J, Seyfarth M, Meyer RC, Willmitzer L & Altmann T (2016) A naturally occurring promoter polymorphism of the Arabidopsis FUM2 gene causes expression variation, and is associated with metabolic and growth traits. *Plant J* **88**, 826–838.
50 Kim SH & Lee WS (2002) Participation of extracellular fumarase in the utilization of malate in cultured carrot cells. *Plant Cell Rep* **20**, 1087–1092.
51 Pedersen AG & Nielsen H (1997) Neural network prediction of translation initiation sites in eukaryotes: perspectives for EST and genome analysis. *Proc Int Conf Intell Syst Mol Biol* **5**, 226–233.
52 Claros MG & Vincens P (1996) Computational method to predict mitochondrially imported proteins and their targeting sequences. *Eur J Biochem* **241**, 779–786.
53 Emanuelsson O, Nielsen H, Brunak S & von Heijne G (2000) Predicting subcellular localization of proteins based on their N-terminal amino acid sequence. *J Mol Biol* **300**, 1005–1016.
54 Petersen TN, Brunak S, von Heijne G & Nielsen H (2011) SignalP 4.0: discriminating signal peptides from transmembrane regions. *Nat Methods* **8**, 785–786.
55 Edgar RC (2004) MUSCLE: multiple sequence alignment with high accuracy and high throughput. *Nucleic Acids Res* **32**, 1792–1797.
56 Ronquist F, Teslenko M, van der Mark P, Ayres DL, Darling A, Höhna S, Larget B, Liu L, Suchard MA & Huelsenbeck JP (2012) MrBayes 3.2: efficient Bayesian phylogenetic inference and model choice across a large model space. *Syst Biol* **61**, 539–542.
57 Wang J, Tao F, Marowsky NC & Fan C (2016) Evolutionary fates and dynamic functionalization of young duplicate genes in arabidopsis genomes. *Plant Physiol* **172**, 427–440.
58 Duarte JM, Wall PK, Edger PP, Landherr LL, Ma H, Pires JC, Leebens-Mack J & dePamphilis CW (2010) Identification of shared single copy nuclear genes in Arabidopsis, Populus, Vitis and Oryza and their phylogenetic utility across various taxonomic levels. *BMC Evol Biol* **10**, 61.
59 Han F, Peng Y, Xu L & Xiao P (2014) Identification, characterization, and utilization of single copy genes in 29 angiosperm genomes. *BMC Genom* **15**, 504.
60 Tamura K, Stecher G, Peterson D, Filipski A & Kumar S (2013) MEGA6: molecular evolutionary genetics analysis version 6.0. *Mol Biol Evol* **30**, 2725–2729.
61 Detarsio E, Wheeler MC, Campos Bermudez VA, Andreo CS & Drincovich MF (2003) Maize C4 NADP-malic enzyme. Expression in *Escherichia coli* and characterization of site-directed mutants at the putative nucleoside-binding sites. *J Biol Chem* **278**, 13757–13764.
62 Annett RG & Kosicki GW (1969) ICeto-Enol tautomerase. *J Biol Chem* **244**, 2059–2067.
63 Laemmly UK (1970) Cleavage of structural proteins during the assembly of the head of bacteriophage T4. *Nature* **227**, 680–685.

Supporting information

Additional Supporting Information may be found online in the supporting information section at the end of the article.

Fig. S1. Alignment of the N-terminal region of plant FUM sequences.

Table S1. Codon-based evolutionary divergence estimation among sequences.

Table S2. Regulatory properties of AtFUM1 and 2 at pH 7.2.

Table S3. Identified tryptic peptides of reAtFUM2 (A) and oxAFUM2 (B) by LC–MS.

Table S4. Accession number of FUM sequences used in this work.